A Multi-Configurational Wave Function Theoretical Study on Electronic Structure and Magnetic Susceptibility of Dilanthanide Single Molecule Magnet

Yue Chen[1]， Ray Miyazaki[1], Shigeyoshi Sakaki[2]， and Jun-ya Hasegawa[1,3]*

[1] Institute for Catalysis, Hokkaido University, N21W10, Kita-ku, Sapporo 001-0021, Japan

[2] Institute for Cell-Material Sciences, Kyoto University, Rhom Plaza, Kyoto-daigaku Katsura, Nishikyo-ku, Kyoto 615-8146, Japan

[3] Interdisciplinary Research Center for Catalytic Chemistry, National Institute of Advanced Industrial Science and Technology, Tsukuba 305-8565, Japan

E-mail: hasegawa@cat.hokudai.ac.jp

ABSTRACT

Single molecule magnet (SMM) has been a promising material for next-generation high-density information storage and molecular spintronics. N_2^{3-}-bridged dilanthanide complexes, $\{[(Me_3Si)_2N]_2Ln(THF)(\mu\text{-}\eta^2\text{:}\eta^2\text{-}N_2)(THF)Ln[(Me_3Si)_2N]_2\}^{1-}$, exhibit high blocking temperature and has been one of the promising candidates for future application. Rational understanding should be established between magnetic properties and electronic structure. However, theoretical study is still challenging due to the complexities in their electronic structures. Here, we theoretically studied the magnetic susceptibility of dilanthanide SMMs based on the state-of-the-art Multi-State-Complete Active Space self-consistent field and Perturbation Theory at 2nd order (MS-CASPT2) and Restricted Active Space State-Interaction with Spin-Orbit Coupling (RASSI-SOC) calculations. Temperature dependence of magnetic susceptibility ($\chi_m T - T$ curve) was quantitatively reproduced by the theoretical calculations. The complexities in the electronic states of these dilanthanide complexes originate from significantly strong static electron correlations in the lanthanide 4f and N_2 π^* orbitals and SOC effect. The temperature dependense of the magnetic susceptibility results from the energy levels and magnetic properties of the low-lying excited state. The $\chi_m T$ values below 50 K are dominated by the ground state, while thermal distribution in the low-lying excited state affects the $\chi_m T$ values over 50 K. Saturation magnetization at low temperature was also evaluated, and the result agrees with the experimental observation.

1. Introduction

Discovery of slow magnetic relaxation of Mn_{12}-acetate cluster opens the door to single-molecule magnets (SMM) that are very attractive for potential application in next-generation high-density information storage and molecular spintronics.[1] Though a number of SMMs have been synthesized over the past two decades, realization of SMM with high blocking temperature (the temperature at which magnetic information is lost within a certain time threshold) of magnetic hysteresis is still a grand challenge.[2-3]

A certain amount of spin reversal energy barrier $\boldsymbol{U}$ is essential for the magnetic property of SMM, which can be estimated by total spin $\boldsymbol{S}$ and axial anisotropy $\boldsymbol{D}$ via $\boldsymbol{U}=|\boldsymbol{D}|\boldsymbol{S}^2$. One strategy to improve $\boldsymbol{U}$ is maximizing the total spin $\boldsymbol{S}$ by synthesis of multinuclear clusters. However, the $\boldsymbol{U}$ values of multi-nuclear clusters do not increase notably due to accompanying low $\boldsymbol{D}$ value.[4-8]

In recent years, considerable attention has been focused on lanthanide SMM because the strong spin-orbit coupling (SOC) of lanthanide can produce high anisotropy.[9] In 2003, Ishikawa et al. developed the first mono-lanthanide SMM $[LnPc_2]^n$ (Ln = Tb^{3+} and Dy^{3+}; H_2Pc = free-base phthalocyanine; n = ±1, 0) which presents greater $\boldsymbol{U}$ value (260 cm^{-1}) than the 3*d*-SMM reported at that time.[10-11] Since then, lots of mono- and polymetallic lanthanide SMMs with large $\boldsymbol{U}$ have been reported.[2, 12-23] From the data collected by recent review,[2] however, SMM with larger $\boldsymbol{U}$ does not definitely show higher block temperature.

Ishikawa et al.[24-25] proposed a nuclear spin coupled model for quantum tunneling effect (QTE) and well reproduced the step-structure and fast magnetization relaxation of $[LnPc_2]^{1-}$. Theoretical investigations on the exchange interaction among magnetic centers and anisotropic properties of lanthanide SMMs are pioneered by Chibotaru,[26-28] Rajaraman,[29-30] Sessoli,[31-32] and Gao[33-34] et al. using density functional theory(DFT), ab initio multiconfigurational wave function theory, and Lines model[35] using properties of mononuclear fragments. However, for lanthanide SMM with multiple magnetic centers, it is still difficult but necessary to reveal the relationship between magnetic properties and electronic structure of entire molecule. There are several essential points to which theoretical contributions are necessary. Among them, a quantitative computational approach for the simulation of magnetic susceptibility $\chi_m T$ should be established. This also helps to establish to interpret the magnetic properties in terms of the molecular and electronic structures.

In this work, we theoretically studied the N_2^{3-}-radical-bridged dilanthanide complexes $\{[(Me_3Si)_2N]_2Ln(THF)(\mu\text{-}\eta^2\text{:}\eta^2\text{-}N_2)(THF)Ln[(Me_3Si)_2N]_2\}^{1-}$ (abbreviated as $[Ln(N_2)Ln]^{1-}$, Ln=Gd (**1**),

Tb (**2**), Dy (**3**)) reported by Long et al., because **2** and **3** are regarded as one of the most susscesful SMMs with high block temperature (14.0 and 8.3 K)[12-13] (See Figure 1 for chemical structure). Complexes **2** and **3** have three magnetic centers and exhibit smooth hysteresis whitin broad range of external magnetic field. Based on electronic structure calculations, we successfully reproduced the magnetic properties, including DC magnetic susceptibility and saturation magnetization, and found that the lowest spin-orbit state contributes dominantly at low temparatures.

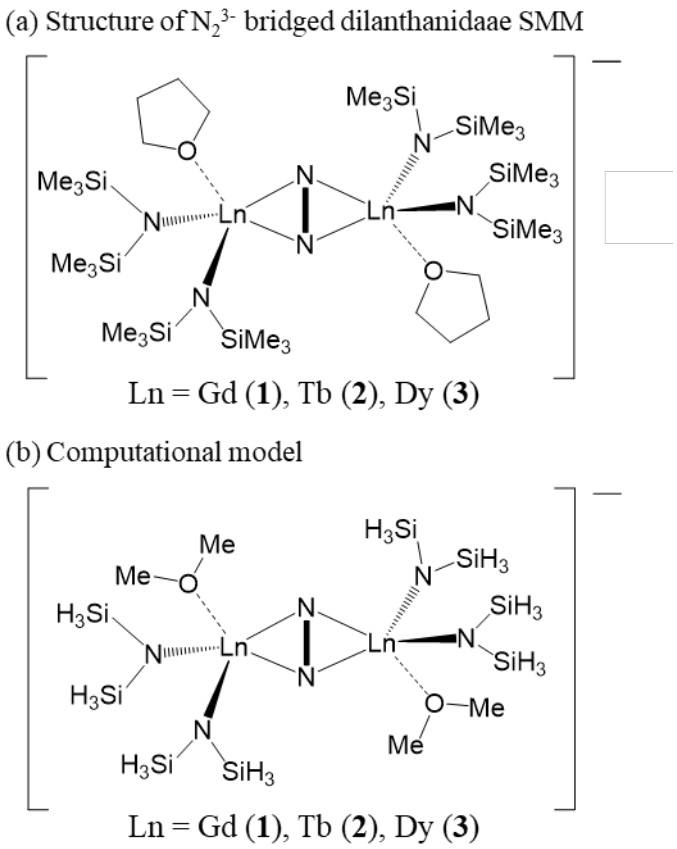

Figure 1. (a) The real complex and (b) a simplified computational model of N_2^{3-} bridged dilanthanide SMM.

2. Computational details

In geometry optimization by DFT functionals, the tetrahydrofuran is replaced by dimethyl ester and the Me_3Si are replaced by H_3Si; see Figure 1. This simplification does not affect the structure of the complexes as compared with X-ray crystallographic structures[12-13]. The basis set (10,10,10,11/88111/6111/611) with ECP proposed by Stuttgart-Dresden-Bonn group was used for Ln, cc-pVTZ without *f* for bridge-N atom, and cc-pVDZ for other N, C, O, Si, and H (abbreviated as BS-I). The

geometry of the Gd complex was optimized by seven DFT functionals (B3LYP,[36-37] mPW1PW91,[38] M06HF,[39-40] BHandHLYP,[37] B3PW91,[36-37, 41] CAM-B3LYP,[42] ωB97X,[43] and BHandH[37]) with C_i symmetry. Though most of the functional worked properly, the geometry optmized by BHandHLYP is the closest to the experimental structure[12-13]; see Table S1(A) in Supplementary information (SI). In addition, geometries of the Tb and Dy complexes optimized at the BHandHLYP/BS-I level also agree well with their experimental structures[12-13]; see Table S1(B). All the DFT calculations are carried out by Gaussian 09 program,[44]

In the CASSCF calculation, the above mentioned DFT optimized structures were used. For the initial guess, natural orbitals obtained by unrestricted Hartree-Fock calculations were employed. We initially examined an active space composed of 14 f-orbitals of two Ln atoms and two π* orbitals of N_2; see Figure S2 in SI. The CASSCF calculations using this active space show that π_z^* orbital (φ_{9a_g}) is always doubly occupied. With this result, the π_z^* orbital of N_2 was excluded, and 15 orbitals were used. The basis set (14,14,14/10,10/10,10/8) with core-AIMP proposed by Seijo[45] was used for Ln, and cc-pVTZ without f-functions for bridge-N atom, and (31/31) with ECP for Si,[46] and (41) for H, and cc-pVDZ for others (abbreviated as BS-II). For each spin-multiplicity, 10 states (5 A_g and 5 A_u states) were obtained, and they are equally weighted in the state-averaged CASSCF calculation. This computational set-up includes 80, 70, and 60 states for **1**, **2**, and **3**, respectively. In Multi-State (MS)-CASPT2 calculations, low-lying 12 orbitals (1s orbitals of C, N, and O atoms) were frozen. To avoide the intruder state problem, the imaginary level shift[47] of 0.1 a.u. was applied. Relative energy at the MS-CASPT2 level for **1**, **2**, and **3** was presented in Table S2. We also adopted the original structure shown in Figure 1a to examine the effect of the simplication in the computational model. The result in Figure S3(D) shows that the simplification does not significantly affect the relative energy levels. In CASSCF and CASPT2 calculations for the $^{14}A_u$, $^{12}A_g$, and $^{10}A_u$ states of **1**, the present simplication introduced root mean square deviation (RMSD) of 0.14 kcal/mol and 1.45 kcal/mol, respectively. In CASPT2 calculations, the deviation arose from high-lying excited states that have minor effect in evaluating Boltzman contributions. Negligible changes were observed in the energy levels of the lowest states. In spin-orbit coupling (SOC) calculations, 15 orbitals (14 f-orbitals and one π* orbital of N_2) are inclued in the active space for all these complexes with different spin states. Thus, the 16-tet state of Gd complexes was not considered in the SOC calculation. This is a safe approximation because of very small SOC in **1**. Restricted active space state interaction (RASSI) method[48-49] together with atomic mean field integrals (AMFI)[50] was used for includinng SOC at the MS-CASPT2 level. Ten spin-free states in each doublet, quartet, sextet, octate, dectet, 12-tet, and 14-tet spin multiplicities were included for **1**. In the same way, doublet to 14-tet states and doublet to 12-tet states were iculded in the wave functions of **2** and **3**, respectively. Magenetic properties, g-tensor, magnetic

moment, and magnetic susceptibility were calculated using the RASSI code.[51] Zeeman Hamiltonian was diagonalized and the resulttant eigenstates were used for calculating magnetization components. MS-CASPT2/CASSCF-SO calculations were carried out by MOLCAS 7.8 program.[52-53]

In calculating the exchange coupling constant (J), a spin hamiltonian, which was used in experimental study,[12] was adopted.

$$\hat{H} = -2J\hat{S}_{radical} \cdot \left(\hat{S}_{Ln1} + \hat{S}_{Ln2}\right) - N_{nn}J'\langle S_z\rangle S_z \quad (1)$$

Spin operators, $\hat{S}_{radical}$ is defined for the N_2^{3-} radical unit, and $\hat{S}_{Ln1}$ and $\hat{S}_{Ln2}$ are defined for two Lanthanide atoms, respectively. Intermolecular exchange coupling constant (J') is multiplied by number of nearest-neighbour molecules (N_{nn}) and z component of spin operator (S_z). Since our computational model is an isolated system, this second term was omitted due to $N_{nn} = 0$. Therefore, constant J' was not calculated.

3. Results and discussion

3-1. Electronic states of dilanthanide complexes

In $[Ln(N_2)Ln]^{1-}$, three spin centers such as two Ln^{3+} and N_2^{3-} can couple into two important spin states, ferromagnetic coupling state **(Ferro)** and ferrimagnetic coupling state **(Ferri)**, as schematically drawn in Figure 2. Gd(III) has a f^7 configuration, and the **Ferro** and **Ferri** states are 16-tet and 14-tet, respectively. In experimental study[13], observed magnetic susceptibility for **1** suggests S_z = 13/2 indicating that **Ferri** state is the ground state. Unrestricted DFT calculations were performed with simplified models shown in Figure 1. The expectation value $\langle\hat{S}^2\rangle$ was 49.78 for **Feeri** of **1**, whih is close to the correct number (48.75) . BHandHLYP functional,[37] which exhibited the best performance for geometry optimization among the DFT functionals (see Table S1A), show that the optimized geometries of **Ferro** and **Ferri** differ little in all three complexes, and both of them agree well with the experimental structure (see Table S1B for geometries). Single-point MS-CASPT2/CASSCF calculations using the DFT optimized structures show that **Ferri** is more stable than **Ferro** by 0.94, 1.43, and 0.76 kcal/mol for **1**, **2**, and **3**, respectively (see Table S3 for the energy). Our results are consistent with experimental observation[12]. In **Ferri**, CASSCF calculations show that Mulliken spin population on N_2 moiety are -0.81, -0.79, and -0.76, for **1**, **2**, and **3**, respectively, (see Table 1) which is consistent with previous DFT calculations.[30, 34] Oppositely, the Gd, Tb, and Dy sites have positive spin population, 6.91, 5.90, and 4.88, respectively. Calculated exchange

coupling constant (-23.4 cm^{-1}) between Gd^{3+} and N_2^{3-} agrees well with the experimental value (-27 cm^{-1}).[12] These results suggest that Ln^{3+} and N_2^{3-} site have antiferromagnetic coupling.

Table 1. The Mulliken spin population of Ln and N_2 moieties in the ground state

	Ground state	Ln	N_2
$Gd(N_2)Gd$	$X^{14}Au$	6.91	-0.81
$Tb(N_2)Tb$	$X^{12}Ag$	5.90	-0.79
$Dy(N_2)Dy$	$X^{10}Au$	4.88	-0.76

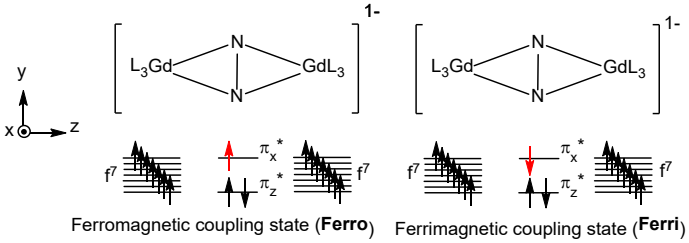

Figure 2. Electronic configuration of **Ferro** and **Ferri** of **1**. The distribution of f-electrons in Gd atoms are schematically drawn. The electronic configuration of Tb and Dy atoms in **2** and **3** is f^8 and f^9, respectively. The y and z directions are parallel to approximate Ln-N-N-Ln molecular plane. The x direction is parpendicular to the plane.

According to the result of MS-CASPT2 calculations, **Ferro** and **Ferri** of these complexes exihbit significant multi-reference character in the wave function except **Ferro** of **1**. In the lowest $X^{14}A_u$ state of **1**, which corresponds to **Ferri**, two configurations $\varphi^2_{3a_g}\varphi^0_{8a_g}$ and $\varphi^0_{3a_g}\varphi^2_{8a_g}$ are dominant configurations with the weight of 23% and 17%, respectively. Other active orbitals are singly occupied by the electron with α spin. The φ_{3a_g} orbital has a weakly anti-bonding interaction between the Ln_2 $\delta_{f_{xyz}}$ orbital and N_2 π_x^* orbital, and the φ_{8a_g} orbital is a counterpart bonding orbital; see Figure 3a. These two configurations are interpreted as biradial character; one electron is in the Ln_2 $\delta_{f_{xyz}}$ orbital and the other electron with opposite spin in N_2 π_x^* orbital. This is proved by natural spin orbitals in which the Ln_2 $\delta_{f_{xyz}}$ orbital and the N_2 π_x^* orbital are occupied by 1.00 α spin electron and 0.93 β spin electron, respectively as shown in Figure 3b. The δ-type interaction is crucial to the stability of $X^{14}A_u$ and expected to be responsible for the SMM behavior. These results indicate quasi-degeneracy arising from interactions between f_{xyz} of Gd and π_x^* of N_2 moiety.

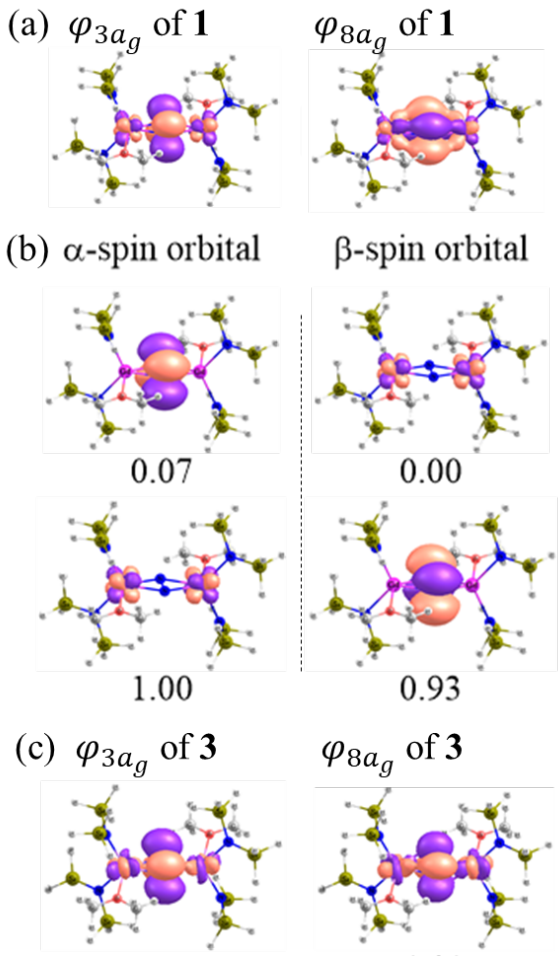

Figure 3. (a) φ_{3a_g} and φ_{8a_g} orbitals obtained for the $X^{14}A_u$ state of **1**. See Figure S2(a) for all the orbitals. (b) Some natural spin orbitals for the $X^{14}A_u$ state of **1**. Those related to the Ln_2 $\delta_{f_{xyz}}$ orbital and the N_2 π_x^* orbital are shown. (c) φ_{3a_g} and φ_{8a_g} orbitals obtained for the $X^{10}A_g$ state of **3**. See Figure S2(c) for all the orbitals.

In $^{14}A_g$ state, there is no dominant configuration with weight more than 7%, but 24 configurations have coefficients with weight more than 2%. They are composed of $\varphi_{ia_g}^2\varphi_{ia_u}^0$ and $\varphi_{ia_g}^0\varphi_{ia_u}^2$ (i = 1-7) types where the φ_{ia_g} and φ_{ia_u} are mainly composed of the Gd *f* orbitals. Other active orbitals are singly occupied. The $^{16}A_u$ state has one main configuration with weight of nearly 100%, in which π_z^* (φ_{8a_g}) are doubly occupied, π_x^* (φ_{9a_g}) is singly occupied, and the rest of the Gd *f* orbitals are singly occupied. This state is a well-known high-spin coupled **Ferro** state.

Though Tb(III) has one more electron than Gd(III), the Tb complex has more complicated electronic structures than the Gd(III) complex. Like the Gd complex, the ground state of Tb complex is **Ferri** ($X^{12}A_u$). Similar to the ground state $X^{14}A_u$ of Gd complex, there is no dominant configuration in $X^{12}A_u$ of Tb complex, but pairs of configurations which include $\varphi_{3a_g}^2\varphi_{8a_g}^0$ and $\varphi_{3a_g}^0\varphi_{8a_g}^2$ occupations have relatively large weight in the wavefunction. This result also indicates important role of the interaction (φ_{3a_g} and φ_{8a_g}) between f_{xyz} of Tb and π_z^* of N_2 moiety. The lowest-lying seven excited states are located within 0.5 kcal/mol above the ground $X^{12}A_u$ state, as shown in Table S2(B) and Figure S3. The lowest excited states $^{10}A_g$ is 0.14 kcal/mol above the ground state.

The ground state of Dy complex **3** is also **Ferri** ($X^{10}A_g$). The energies of all calculated 60 excited states are within 1.2 kcal/mol relative to the ground state. Because the number of configuration increases singnificantly compared with Gd and Tb complexes, none of the configurations contributes more than 7% to the ground state. Different from the ground states of Gd and Dy complexes, there is no bonding overlap between f_{xyz} of Dy and π_x^* of N_2 moiety but the overlap is observed between f_{yz^2} of Dy and π_x^* of N_2 as shown in Figure 3c.

3-2. Magnetic property of dilanthanide complexes

Firstly, we calculated the magnetic susceptibility $\chi_m T$ from 1.0 to 300.0 K using spin components of spin-free MS-CASPT2 states with Boltzmann population in field of 1.0 Tesla.

$$\chi_m = \frac{M}{H} = \frac{N_a \sum \mu_i p_i}{H} \quad (2)$$

where M is molar magnetization, H is strength of external magnetic field, N_a is Avogadro's number, μ_i ($= \mu_B g_e M_s$) is magnetic moment of the spin-free state (i), μ_B is Bohr magnetron constant, g_e (= 2.0023) is g-factor, M_s is spin quantum number of the state, and p_i is the Boltzmann population. This means a part of magnetic moment which originates from orbital angular moment was not included. See Table S2 (A) for the energy of low-lying 80 spin-free states of the Gd complex **1** calculated with MS-CASPT2. For instance, a $^{14}A_u$ state provides 14 spin components with different spin angular momentum, and the 14 states are degenerate under zero magnetic field. The $\chi_m T - T$ curve of **1** shows a peak value of 24.3 emu•K/mol at a lower temperature (26 K), which is quantitatively close to the experimental value (23.9 emu•K/mol) as shown by a green line in Figure 4(a). In contrast, the $\chi_m T$ value at 300 K (12.0 emu•K/mol) is smaller than the experimental data (15.3 emu•K/mol).

To examine how many states are necessary to reproduce the result with 80 states for **1**, we picked up several low lying spin-free states and calculated the $\chi_m T - T$ curve. At lower temperature, the ground state contributes dominantly to the $\chi_m T - T$ curve as shown in the left side of the curve in Figure 4(b).

In contrast, at higher temperatures, more spin-free states are necessary to reach a converging $\chi_m T$ value as seen in the right side of the curve in Figure 4(b). This feature results from the contribution of the spin-free states with small spin-multiplicities as seen in Table S2(A). These results indicate the ground state exhibits the main responsibility at low temperatures upto 25 K, but the contributions from low-lying excited states with small magnetic moment become more prominent at temparatures closer to the room temparature.

In contrast to the Gd complex **1**, the $\chi_m T - T$ curves of the Tb complex **2** and the Dy complex **3** calculated with the spin components of spin-free states seriously deviate from experimental observations.[12-13] As seen in Figure 4(a), calculated $\chi_m T$ valuses for **2** and **3** at low temperature are 17.7 emu•K/mol and 12.2 emu•K/mol, while corresponding experimental values are 34.5 emu•K/mol and 42.5 emu•K/mol, respectively.

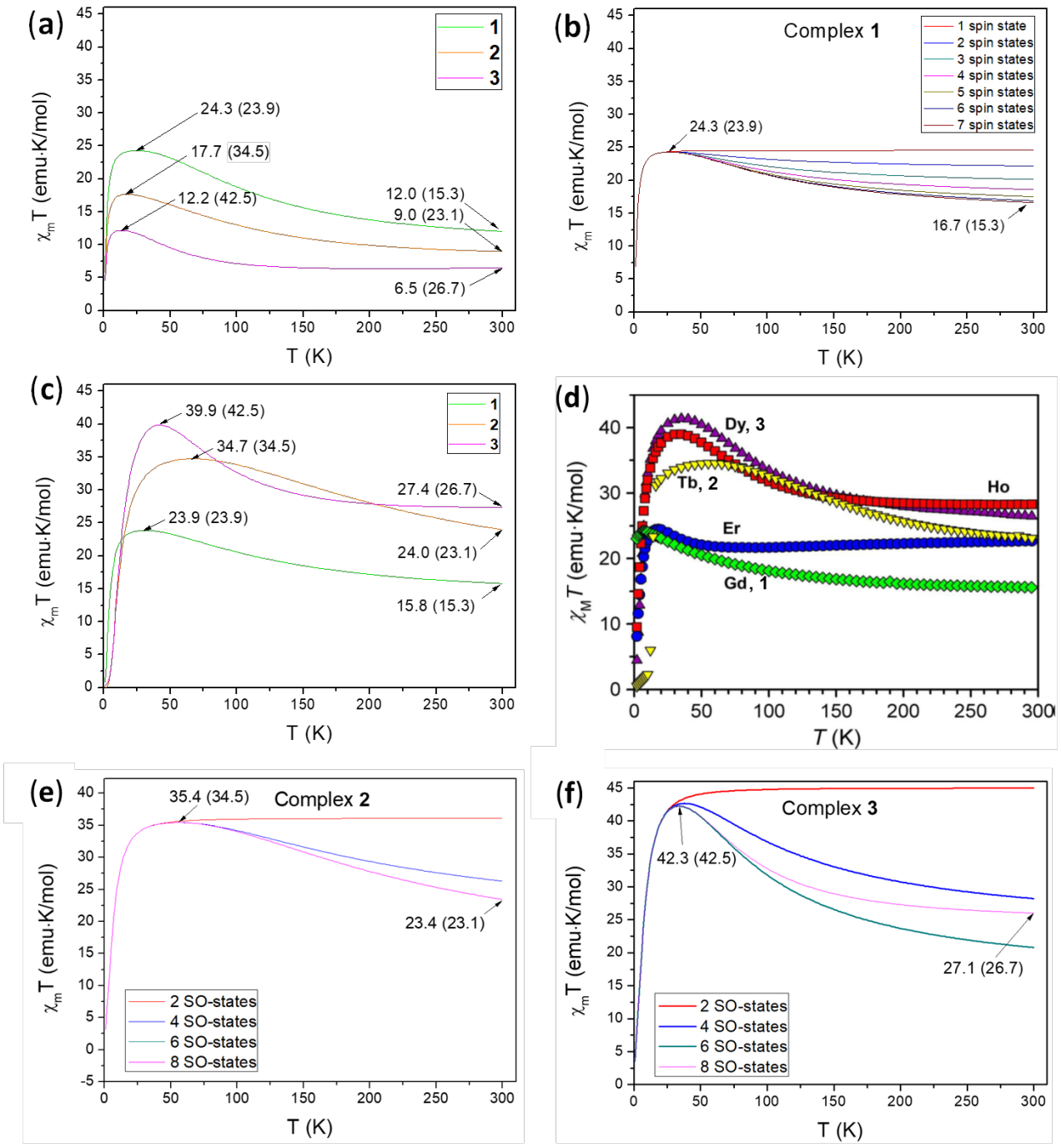

Figure 4. (a) Magnetic susceptibility simulated with 80 spin states listed in Table S2A with Boltzmann population under 1.0 Tesla field. (b) The magnetic susceptibility of the Gd complex **1** simulated by 1-7 lowest spin states. (c) The $\chi_m T - T$ curves are calculated by using magnetic moment of the eigenstates of spin-orbit Hamiltonian (Zeeman states). (d) Experimentally measured $\chi_m T - T$ curves reprinted from Ref. 13 Copyright 2011 American Chemical Society. (e, f) The $\chi_m T - T$ curves calculated by using the magnetic moment of 2-8 SO-states for **2** and **3**, respectively. The $\chi_m T$ value at peak and 300 K are shown, and corresponding experimental value is also shown in parenthesis. In (e), the curves with 6 SO-states and 8 SO-states almost completely overlap because of the large energy gap between SO-state 5(6) and SO-state 7(8); see Table 2. In these calculations, the external field is set to 1 Tesla.

Such deviation would be attributed to no SOC effect into the energy and wave function and also to no f-orbital angular moment included into total magnetic moment in eq. 2. Then, we calculated the magnetic susceptibility using the eigenstates of Zeeman Hamiltonian[51] in temperature range 1-300 K by means of RASSI-SOC method[49] and making use of AMFI integrals.[50] Caluclated $\chi_m T - T$ curves of all these complexes agree very well with experimental curves; see Figure 4c. Experimental curves[13] are also shown in Figure 4d. The experimental peak values at lower temperature of **1**, **2**, and **3** (23.8 emu•K/mol at 9 K, 34.5 emu•K/mol at 55 K, and 42.5 emu•K/mol at 25 K) are qualitatively reproduced by our calculation (23.9 emu•K/mol at 39 K, 34.7 emu•K/mol at 67 K, and 39.9 emu•K/mol at 42 K), respectively. At 300K, the calculated $\chi_m T$ values are 15.8, 24.0, and 27.4 emu•K/mol for **1**, **2**, and **3**, respectively, which are close to corresponding experimental values, 15.3, 23.1, and 26.7 emu•K/mol. These results indicate that the state-of-the-art calulation with SOC is a requisite condition for the quantitative description of magnetic suspetibility of the lanthanide dimer complexes. Here, we checked the results at very low temperature because the lowest-energy state gives the dominant contribution to the property. It should be noted that a relatively large deviation was observed in the peak value of **3** at very low temperatures. This deviation suggests that both degeneracy in the electronic configurations and spin-orbit interactions become more challening problems as the number of 4f electron increases, as discussed above.

In Table 2, energy levels of the ground and excited states of **2** an **3** calculated with the RASSI-SO method are summarized. For the Gd complex **1**, SOC is negligiblly small; indeed, the computational results were very similar to those by MS-CASPT2 calculations without SOC, as shown in Table S2A. As shown in Figure 2, the wave function of **1** is composed of electron configurations with singly-occupied fourteen 4f orbitals. Since this electron occupation is unique among the states in the neighboring spin-multiplicity, the SOC becomes so small in the complex **1**. Spin-orbit Hamiltonian matrix elements between the spin-free CASSCF states are at most sub cm^{-1} order. For example, the coupling in **1** is only 0.3 cm^{-1} between the $1^{14}A_g$ state and $1^{12}A_g$ state. The ground and excited states of **2** and **3** are eigenstates of the SO Hamiltonian (hereafter, we call as SO-state) and are doubly degenerate in energy, Kramers pair. The wave function is represented by the linear combination of the spin-free MS-CASPT2 wave functions. In the case of **2**, the lowest-energy pair of SO-states is composed of 12-tet states, and the dominant component is 1^{12}Ag state that has weight of 51%. The SOC introduces a component of 14-tet state, but the weight is very limited. The SO-states 3 and 4, which are next lowest, are composed of 2^4A_g state but the weight is only 21%. In the case of **3**, the ground SO-state is mainly composed of $2^{10}A_u$ state. The SO-

states 3 and 4 consists of 4^4A_g state, but non negligible amount of doublet, sextet, and octet components were found.

To investigate the effect of the thermal mixing among the SO-states and its effect to the magnetic susceptibility, the $\chi_m T - T$ curves were simulated with eq. (2) by using limited number of the SO states. To calculate magnetic moment, the molecular g factors were obtained with approarch II in ref. 54, in which the Zeeman effect was included through the first-order degenerate perturbation theory within Kramers doublet. External magnetic field of 1 T was applied. In Table 3, calculated g-factors for the SO-states of **2** and **3** are summarized. The results of the $\chi_m T - T$ curve for **2** and **3** was shown in Figures 4e and 4f, respectively. In case that only the ground SO-states was used, the calculated $\chi_m T - T$ curve shows a rapid increase when temperature is below 50 K, and the curve keeps the high $\chi_m T$ values when temperatures is up to 300K. This feature is apparently different from the experimental one in Figure 4d and from the calculated one in Figure 4c. The temperature dependence significantly changes if the next lowest-energy pair of SO-states were included. The $\chi_m T$ value declines with temperatures over 50 K as observed in the experiment. This indicates that the SO states 3 to 4 with small g-factors (see Table 3) are populated. The $\chi_m T$ value more decreases after the inclusion of the SO-states 5 and 6 which also have small g-factor. Further inclusion of the SO-states 7 and 8 raises the $\chi_m T - T$ curve also due to the large g-value. The same interpretation can be applied to the Dy complex **3**. According to Tables 3 and S2A, the energy gap ($E_{1\text{-}0}$) between the first excited SO/spin state and ground SO/spin state decreases in the order **2** (204 cm^{-1}) > **3** (106 cm^{-1}) > **1** (84 cm^{-1}). This result indicates that the $\chi_m T - T$ curve of **1** delines at the lowest temparature in these complexes, that of **3** next, and that of **2** at the highest temperature. These results agree with the experimenal $\chi_m T - T$ curve as shown in Figure 4d, in which the peak temerature increases in the order **1** (9 K) < **3** (25 K) < **2** (55 K). Therefore, it is concluded that the shape of the experimental $\chi_m T - T$ curve results from the Boltzman distribution of the low-lying excited SO-states.

Table 2. The energies and wave function component of low-lying eigenstates (SO state) of spin-orbit Hamiltonian for complexes **2** and **3**.

SO state[a]	E (cm^{-1}/ kcal mol^{-1})	Components (MS-CASPT2 states)
		Complex **2**
1 and 2	0 / 0.00	51.0% $1^{12}A_g$ + 24.7% $2^{12}A_g$ + 16.8% $4^{12}A_g$ + 7.4% $3^{12}A_g$ + 0.1% $1^{14}A_g$
3 and 4	204 / 0.58	21.0% $2^{4}A_g$ + 13.7% $1^{2}A_g$ + 9.8% $1^{6}A_g$ + 8.2% $3^{6}A_g$ + 7.7% $5^{6}A_g$
5 and 6	369 / 1.06	21.1% $1^{4}A_u$ + 15.6% $2^{2}A_u$ + 8.5% $2^{6}A_u$ + 8.4% $4^{4}A_u$ + 8.2% $5^{4}A_u$
7 and 8	1587 / 4.54	50.4% $1^{10}A_u$ + 24.3% $4^{10}A_u$ + 17.5% $2^{10}A_u$ + 6.3% $3^{10}A_u$ + 0.8% $2^{12}A_u$
		Complex **3**
1 and 2	0 / 0.0	44.1% $2^{10}A_u$ + 27.0% $1^{10}A_u$ + 20.7% $3^{10}A_u$ + 3.9% $2^{12}A_u$ + 2.2% $1^{12}A_u$
3 and 4	106 / 0.30	20.6% $4^{4}A_g$ + 12.2% $1^{2}A_g$ + 8.2% $2^{6}A_g$ + 7.5% $4^{8}A_g$ +7.1% $4^{2}A_g$
5 and 6	113 / 0.32	14.5% $5^{2}A_u$ + 13.9% $5^{6}A_u$ + 12.8% $3^{4}A_u$ + 12.4% $1^{4}A_u$ + 10.5% $4^{4}A_u$
7 and 8	193 / 0.55	47.9% $2^{12}A_u$ + 27.1% $1^{12}A_u$ + 23.4% $3^{12}A_u$ + 0.8% $5^{12}A_u$ + 0.7% $4^{12}A_u$

[a] A pair of degenerated states, Kramers pair.

Table 3. Calculated g-factor of the low-lying SO states of complexes **2** and **3**.

SO state[a]	g_1	g_2	g_3
		Complex **2**	
1 and 2	33.9039	0.0000	0.0000
3 and 4	2.0135	0.5743	0.5602
5 and 6	2.0190	1.0634	1.0403
7 and 8	29.8539	0.0000	0.0000
		Complex **3**	
1 and 2	37.8538	0.0000	0.0000
3 and 4	2.1195	1.7639	1.8363
5 and 6	2.1297	1.7451	1.8599
7 and 8	41.8307	0.0000	0.0000

In magnetic hysteresis loop, powder samples exhibit saturation magnetization (M_{sat}) at the maximum filed B_{max} (or $-B_{\mathrm{max}}$), as illustrated in Figure S5. Considering random orientation of molecules in powder sample, component of magnetic moment(μ_{m}) along the external field is $\mu_{\mathrm{m}}\cos\theta$,

where θ is the angle between the external field and magnetic moment. The total magnetization along external field is calculated to be $(1/2)\mu_{\mathrm{m}}$ (see more details in section S5 in SI). This simple relation is useful to estimate M_{sat}. Magnetic moments of **2** and **3** at low temperature regime are calculated to be 16.95 and 18.93 μ_B, respectively, using the relation $\mu_{\mathrm{m}} = (1/2)g_{\parallel}\mu_{\mathrm{B}}$, where $g_{\parallel}$ is the easy axis g-value (see Table 3), the factor of $1/2$ is the effective spin quantum number of Kramer's doublet, and μ_{B} is the Bohr magneton. Then, the powder M_{sat} is 8.48 and 9.47 μ_{B} for **2** and **3**, respectively, which agree well with corresponding experimental data (8.5 and 9.5 μ_{B},[12-13] respectively). Such kind of relationship is also observed in other Lanthanide SMMs,[32, 55] as shown in Table 4.

Table 4. The experimental and calculated saturation magnetization M_{sat} (unit: μ_B)

Complex	Expt.[a]	Calc.
2	8.5[13]	8.48[c]
3	9.5[12]	9.47[c]
$Dy(hfac)_3(NIT\text{-}C_6H_4OEt)_2$	4.8 (9.8)[b,32]	4.40[d]
$Dy(3\text{-}py\text{-}4\text{-}pmc)(C_2O_4)_{0.5}(OH)(H_2O)$	4.9[55]	4.96[e]

[a]Experimental M_{sat} of powder sample is estimated from the reference.

[b]The value in parenthesis is M_{sat} along easy axis.

[c]The $g_{\parallel}$ corresponds to g_1 in Table 3.

[d]The calculated $g_{\parallel}$ value (17.6) is taken from ref. 32.

[e]The calculated $g_{\parallel}$ value (19.8) is taken from ref. 55.

4. Conclusions

MS-CASPT2 calculation followed by RASSI-SOC calculation was applied to temparature dependence of magnetic susceptibility of N_2^{3-} radical bridged dinuclear lanthanide SMM, $\{[(Me_3Si)_2N]_2Ln(THF)(\mu\text{-}\eta^2\text{:}\eta^2\text{-}N_2)(THF)Ln[(Me_3Si)_2N]_2\}^{1-}$ (Ln = Gd(**1**), Tb(**2**), and Dy(**3**).[12-13] Theoretically calculated $\chi_m T - T$ curves quantitatively agree with the experimental data.

Electronic structures of the complexes are complicated with highly multi-configurational character. The configuration interaction shows biradical character which arises from the intemediate spin coupling between the two lanthanide centers and N_2^{3-} bridge. Spin-multiplicity of the ground state in the MS-CASPT2 calculations is 14-tet, 12-tet, and 10-tet for **1**, **2**, and **3**, respectively. SOC mixes spin-free MS-

CASPT2 states within the same spin multiplicity in the ground SO-state wave function, while the spin-free state of the excited states with several different spin-mulitiplicity are coupled in the low-lying excited SO-states. In addition, several low-lying excited SO-states are thermally populated, inducing the influence to the shape of the $\chi_m T - T$ curves. Computational results show that the ground state dominates the $\chi_m T - T$ curve in low temperature region up to 50 K and and play a crucial role in determining the peak value of the $\chi_m T$ values. The present analysis also shows that the decrease of the $\chi_m T$ value over 50 K results from the thermal populations of the next lowest excited states with relatively small magnetic moments.

Saturation magnetization of several lanthanide complexes including 2, 3, and two other Dy complexes was evaluated. Quantitative agreements show that the present computational procedure is useful for evaluation of saturation magnetization.

The present MS-CASPT2 and RASSI-SOC approach successfully works for evaluation of the $\chi_m T - T$ curve for the dilanthanide Gd, Tb, and Dy complexes. Especially, accuracy in the energy levels of the low-lying excited state is essentially important to reproduce temperature dependence of the magnetic susceptibility. A next challenging target is lanthanide with more 4f electrons, because static electron correlations of 4f electrons are expected to be stronger, and therefore, larger active space is necessary for the quantitative calculations.

Supporting Information

The Supporting Information is available free of charge at https://pubs.acs.org/doi/10.1021/****.

The Supporting Information includes, computational models and choice of DFT functional, active space for CASSCF calculations, relative potential energy of the ground and excited states, relative potential energy of **Ferro** and **Ferri** obtained with MS-CASPT2 calculations, saturation magnetization, and cartesian coordinates of the dilanthanide complexes.

Acknowledgements

This study was supported by JSPS KAKENHI (Grant Number 20H02685 and 23K17898). This study was also supported by Photoexcitonix project, Junior Scientist Promotion in Hokkaido University, Joint Usage/Research Center for Catalysis, Integrated Research Consortium on Chemical Sciences. A part

of the computation was performed using Research Center for Computational Science, Okazaki, Japan (Project: 23-IMS-C002).

Reference

1. Sessoli, R.; Gatteschi, D.; Caneschi, A.; Novak, M. A., Magnetic bistability in a metal-ion cluster. *Nature* **1993**, *365*, 141-143.
2. Woodruff, D. N.; Winpenny, R. E. P.; Layfield, R. A., Lanthanide Single-Molecule Magnets. *Chem Rev* **2013**, *113*, 5110-5148.
3. Zabala-Lekuona, A.; Seco, J. M.; Colacio, E., Single-Molecule Magnets: From Mn_{12}-ac to dysprosium metallocenes, a travel in time. *Coord Chem Rev* **2021**, *441*.
4. Ako, A. M.; Hewitt, I. J.; Mereacre, V.; Clérac, R.; Wernsdorfer, W.; Anson, C. E.; Powell, A. K., A Ferromagnetically Coupled Mn_{19} Aggregate with a Record S=83/2 Ground Spin State. *Angew Chem Int Ed* **2006**, *45*, 4926-4929.
5. Milios, C. J.; Vinslava, A.; Wernsdorfer, W.; Moggach, S.; Parsons, S.; Perlepes, S. P.; Christou, G.; Brechin, E. K., A Record Anisotropy Barrier for a Single-Molecule Magnet. *J Am Chem Soc* **2007**, *129*, 2754-2755.
6. Waldmann, O., A Criterion for the Anisotropy Barrier in Single-Molecule Magnets. *Inorg Chem* **2007**, *46*, 10035-10037.
7. Neese, F.; Pantazis, D. A., What is not required to make a single molecule magnet. *Faraday Discussions* **2011**, *148*, 229-238.
8. Christou, G.; Gatteschi, D.; Hendrickson, D. N.; Sessoli, R., Single-Molecule Magnets. *MRS Bulletin* **2000**, *25*, 66-71.
9. Nakano, M.; Oshio, H., Magnetic anisotropies in paramagnetic polynuclear metal complexes. *Chem Soc Rev* **2011**, *40*, 3239-3248.
10. Ishikawa, N.; Sugita, M.; Ishikawa, T.; Koshihara, S.; Kaizu, Y., Lanthanide Double-Decker Complexes Functioning as Magnets at the Single-Molecular Level. *J Am Chem Soc* **2003**, *125*, 8694-8695.
11. Ishikawa, N.; Sugita, M.; Ishikawa, T.; Koshihara, S.; Kaizu, Y., Mononuclear Lanthanide Complexes with a Long Magnetization Relaxation Time at High Temperatures: A New Category of Magnets at the Single-Molecular Level. *J Phys Chem B* **2004**, *108*, 11265-11271.
12. Rinehart, J. D.; Fang, M.; Evans, W. J.; Long, J. R., Strong exchange and magnetic blocking in N_2^{3-}-radical-bridged lanthanide complexes. *Nat Chem* **2011**, *3*, 538-542.
13. Rinehart, J. D.; Fang, M.; Evans, W. J.; Long, J. R., A N_2^{3-} Radical-Bridged Terbium Complex Exhibiting Magnetic Hysteresis at 14 K. *J Am Chem Soc* **2011**, *133*, 14236-14239.
14. Xue, S.; Chen, X.-H.; Zhao, L.; Guo, Y.-N.; Tang, J., Two Bulky-Decorated Triangular Dysprosium Aggregates Conserving Vortex-Spin Structure. *Inorg Chem* **2012**, *51*, 13264-13270.
15. Wang, Y.-X.; Shi, W.; Li, H.; Song, Y.; Fang, L.; Lan, Y.; Powell, A. K.; Wernsdorfer, W.; Ungur, L.; Chibotaru, L. F.; Shen, M.; Cheng, P., A single-molecule magnet assembly exhibiting a dielectric transition at 470 K. *Chem Sci* **2012**, *3*, 3366-3370.
16. Hewitt, I. J.; Lan, Y.; Anson, C. E.; Luzon, J.; Sessoli, R.; Powell, A. K., Opening up a dysprosium triangle by ligand oximation. *Chem Comm* **2009**, 6765-6767.
17. Guo, Y.-N.; Xu, G.-F.; Gamez, P.; Zhao, L.; Lin, S.-Y.; Deng, R.; Tang, J.; Zhang, H.-J., Two-Step Relaxation in a Linear Tetranuclear Dysprosium(III) Aggregate Showing Single-Molecule Magnet Behavior. *J Am Chem Soc* **2010**, *132*, 8538-8539.
18. Anwar, M. U.; Thompson, L. K.; Dawe, L. N.; Habib, F.; Murugesu, M., Predictable self-assembled [2×2] $Ln(III)_4$ square grids (Ln = Dy,Tb)-SMM behaviour in a new lanthanide cluster motif. *Chem Comm* **2012**, *48*, 4576-4578.
19. Blagg, R. J.; Muryn, C. A.; McInnes, E. J. L.; Tuna, F.; Winpenny, R. E. P., Single Pyramid Magnets: Dy_5 Pyramids with Slow Magnetic Relaxation to 40 K. *Angew Chem Int Ed* **2011**, *50*, 6530-6533.
20. Blagg, R. J.; Tuna, F.; McInnes, E. J. L.; Winpenny, R. E. P., Pentametallic lanthanide-alkoxide square-based pyramids: high energy barrier for thermal relaxation in a holmium single molecule magnet. *Chem Comm* **2011**, *47*, 10587-10589.
21. Hewitt, I. J.; Tang, J.; Madhu, N. T.; Anson, C. E.; Lan, Y.; Luzon, J.; Etienne, M.; Sessoli, R.; Powell, A. K., Coupling Dy_3 Triangles Enhances Their Slow Magnetic Relaxation. *Angew Chem Int Ed* **2010**, *49*, 6352-6356.
22. Guo, Y.-N.; Chen, X.-H.; Xue, S.; Tang, J., Molecular Assembly and Magnetic Dynamics of Two Novel Dy_6 and Dy_8 Aggregates. *Inorg Chem* **2012**, *51*, 4035-4042.
23. Branzoli, F.; Carretta, P.; Filibian, M.; Zoppellaro, G.; Graf, M. J.; Galan-Mascaros, J. R.; Fuhr, O.; Brink, S.; Ruben, M., Spin Dynamics in the Negatively Charged Terbium (III) Bis-phthalocyaninato Complex. *J Am Chem Soc* **2009**, *131*, 4387-4396.

24. Ishikawa, N.; Sugita, M.; Wernsdorfer, W., Nuclear Spin Driven Quantum Tunneling of Magnetization in a New Lanthanide Single-Molecule Magnet: Bis(Phthalocyaninato)holmium Anion. *J Am Chem Soc* **2005**, *127*, 3650-3651.
25. Ishikawa, N.; Sugita, M.; Wernsdorfer, W., Quantum Tunneling of Magnetization in Lanthanide Single-Molecule Magnets: Bis(phthalocyaninato)terbium and Bis(phthalocyaninato)dysprosium Anions. *Angew Chem Int Ed* **2005**, *44*, 2931-2935.
26. Chibotaru, L. F.; Ungur, L., Ab initio calculation of anisotropic magnetic properties of complexes. I. Unique definition of pseudospin Hamiltonians and their derivation. *J Phys Chem* **2012**, *137*, 064112.
27. Ungur, L.; Van den Heuvel, W.; Chibotaru, L. F., Ab initio investigation of the non-collinear magnetic structure and the lowest magnetic excitations in dysprosium triangles. *New J Chem* **2009**, *33*, 1224-1230.
28. Blagg, R. J.; Ungur, L.; Tuna, F.; Speak, J.; Comar, P.; Collison, D.; Wernsdorfer, W.; McInnes, E. J. L.; Chibotaru, L. F.; Winpenny, R. E. P., Magnetic relaxation pathways in lanthanide single-molecule magnets. *Nat Chem* **2013**, *5*, 673-678.
29. Singh, S. K.; Rajeshkumar, T.; Chandrasekhar, V.; Rajaraman, G., Theoretical studies on {3d-Gd} and {3d-Gd-3d} complexes: Effect of metal substitution on the effective exchange interaction. *Polyhedron* **2013**, *66*, 81-86.
30. Rajeshkumar, T.; Rajaraman, G., Is a radical bridge a route to strong exchange interactions in lanthanide complexes? A computational examination. *Chem Comm* **2012**, *48*, 7856-7858.
31. Cucinotta, G.; Perfetti, M.; Luzon, J.; Etienne, M.; Car, P.-E.; Caneschi, A.; Calvez, G.; Bernot, K.; Sessoli, R., Magnetic Anisotropy in a Dysprosium/DOTA Single-Molecule Magnet: Beyond Simple Magneto-Structural Correlations. *Angew Chem Int Ed* **2012**, *51*, 1606-1610.
32. Bernot, K.; Luzon, J.; Bogani, L.; Etienne, M.; Sangregorio, C.; Shanmugam, M.; Caneschi, A.; Sessoli, R.; Gatteschi, D., Magnetic Anisotropy of Dysprosium(III) in a Low-Symmetry Environment: A Theoretical and Experimental Investigation. *J Am Chem Soc* **2009**, *131*, 5573-5579.
33. Qian, K.; Baldovi, J. J.; Jiang, S.-D.; Gaita-Arino, A.; Zhang, Y.-Q.; Overgaard, J.; Wang, B.-W.; Coronado, E.; Gao, S., Does the thermal evolution of molecular structures critically affect the magnetic anisotropy? *Chem Sci* **2015**, *6*, 4587-4593.
34. Zhang, Y.-Q.; Luo, C.-L.; Wang, B.-W.; Gao, S., Understanding the Magnetic Anisotropy in a Family of N23–Radical-Bridged Lanthanide Complexes: Density Functional Theory and ab Initio Calculations. *J Phys Chem A* **2013**, *117*, 10873-10880.
35. Lines, M. E., Orbital Angular Momentum in the Theory of Paramagnetic Clusters. *J Phys Chem* **1971**, *55*, 2977-2984.
36. Lee, C.; Yang, W.; Parr, R. G., Development of the Colle-Salvetti correlation-energy formula into a functional of the electron density. *Phys Rev B* **1988**, *37*, 785-789.
37. Becke, A. D., A new mixing of Hartree‐Fock and local density‐functional theories. *J Phys Chem* **1993**, *98*, 1372-1377.
38. Adamo, C.; Barone, V., Exchange functionals with improved long-range behavior and adiabatic connection methods without adjustable parameters: The mPW and mPW1PW models. *J Chem Phys* **1998**, *108*, 664-675.
39. Zhao, Y.; Truhlar, D. G., Comparative DFT study of van der Waals complexes: Rare-gas dimers, alkaline-earth dimers, zinc dimer, and zinc-rare-gas dimers. *J Phys Chem A* **2006**, *110*, 5121-5129.
40. Zhao, Y.; Truhlar, D. G., Density functional for spectroscopy: No long-range self-interaction error, good performance for Rydberg and charge-transfer states, and better performance on average than B3LYP for ground states. *J Phys Chem A* **2006**, *110*, 13126-13130.
41. Perdew, J. P.; Wang, Y., Accurate and Simple Analytic Representation of the Electron-Gas Correlation-Energy. *Phys Rev B* **1992**, *45*, 13244-13249.
42. Yanai, T.; Tew, D. P.; Handy, N. C., A new hybrid exchange-correlation functional using the Coulomb-attenuating method (CAM-B3LYP). *Chem Phys Lett* **2004**, *393*, 51-57.
43. Chai, J. D.; Head-Gordon, M., Optimal operators for Hartree-Fock exchange from long-range corrected hybrid density functionals. *Chem Phys Lett* **2008**, *467*, 176-178.
44. Frisch, M. J.; Trucks, G. W.; Schlegel, H. B.; Scuseria, G. E.; Robb, M. A.; Cheeseman, J. R.; Scalmani, G.; Barone, V.; Mennucci, B.; Petersson, G. A.; Nakatsuji, H.; Caricato, M.; Li, X.; Hratchian, H. P.; Izmaylov, A. F.; Bloino, J.; Zheng, G.; Sonnenberg, J. L.; Hada, M.; Ehara, M.; Toyota, K.; Fukuda, R.; Hasegawa, J.; Ishida, M.; Nakajima, T.; Honda, Y.; Kitao, O.; Nakai, H.; Vreven, T.; Montgomery, J. A.; Peralta, J. E.; Ogliaro, F.; Bearpark, M.; Heyd, J. J.; Brothers, E.; Kudin, K. N.; Staroverov, V. N.; Kobayashi, R.; Normand, J.; Raghavachari, K.; Rendell, A.; Burant, J. C.; Iyengar, S. S.; Tomasi, J.; Cossi, M.; Rega, N.; Millam, J. M.; Klene, M.; Knox, J. E.; Cross, J. B.; Bakken, V.; Adamo, C.; Jaramillo, J.; Gomperts, R.; Stratmann, R. E.; Yazyev, O.; Austin, A. J.; Cammi, R.; Pomelli, C.; Ochterski, J. W.; Martin, R. L.; Morokuma, K.; Zakrzewski, V. G.; Voth, G. A.; Salvador, P.; Dannenberg, J. J.; Dapprich, S.; Daniels, A. D.; Farkas; Foresman, J. B.; Ortiz, J. V.; Cioslowski, J.; Fox, D. J., Gaussian 09, Revision B.01. Wallingford CT, 2010.
45. Seijo, L.; Barandiaran, Z.; Ordejon, A., Transferability of core potentials to f and d states of lanthanide and actinide ions. *Mol Phys* **2003**, *101*, 73-80.
46. Bergner, A.; Dolg, M.; Kuchle, W.; Stoll, H.; Preuss, H., Ab-Initio Energy-Adjusted Pseudopotentials for Elements of Groups 13-17. *Mol Phys* **1993**, *80*, 1431-1441.
47. Forsberg, N.; Malmqvist, P. A., Multiconfiguration perturbation theory with imaginary level shift. *Chem Phys Lett* **1997**, *274*, 196-204.

48. Malmqvist, P. A., Calculation of Transition Density-Matrices by Nonunitary Orbital Transformations. *Int J Quantum Chem* **1986**, *30*, 479-494.
49. Malmqvist, P. Å.; Roos, B. O.; Schimmelpfennig, B., The restricted active space (RAS) state interaction approach with spin–orbit coupling. *Chem Phys Lett* **2002**, *357*, 230-240.
50. Heß, B. A.; Marian, C. M.; Wahlgren, U.; Gropen, O., A mean-field spin-orbit method applicable to correlated wavefunctions. *Chem Phys Lett* **1996**, *251*, 365-371.
51. Vancoillie, S.; Rulíšek, L.; Neese, F.; Pierloot, K., Theoretical Description of the Structure and Magnetic Properties of Nitroxide−Cu(II)−Nitroxide Spin Triads by Means of Multiconfigurational Ab Initio Calculations. *J Phys Chem A* **2009**, *113*, 6149-6157.
52. Karlstrom, G.; Lindh, R.; Malmqvist, P. A.; Roos, B. O.; Ryde, U.; Veryazov, V.; Widmark, P. O.; Cossi, M.; Schimmelpfennig, B.; Neogrady, P.; Seijo, L., MOLCAS: a program package for computational chemistry. *Comp Mater Sci* **2003**, *28*, 222-239.
53. Aquilante, F.; De Vico, L.; Ferre, N.; Ghigo, G.; Malmqvist, P. A.; Neogrady, P.; Pedersen, T. B.; Pitonak, M.; Reiher, M.; Roos, B. O.; Serrano-Andres, L.; Urban, M.; Veryazov, V.; Lindh, R., Software News and Update MOLCAS 7: The Next Generation. *J Comput Chem* **2010**, *31*, 224-247.
54. Vancoillie, S.; Malmqvist, P.-Å.; Pierloot, K., Calculation of EPR g Tensors for Transition-Metal Complexes Based on Multiconfigurational Perturbation Theory (CASPT2). *ChemPhysChem* **2007**, *8*, 1803-1815.
55. Yin, D.-D.; Chen, Q.; Meng, Y.-S.; Sun, H.-L.; Zhang, Y.-Q.; Gao, S., Slow magnetic relaxation in a novel carboxylate/oxalate/hydroxyl bridged dysprosium layer. *Chem Sci* **2015**, *6*, 3095-3101.

Table of Contents Graphics

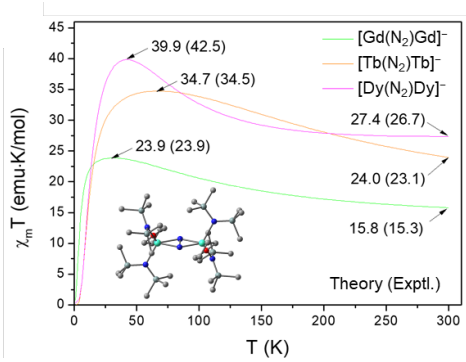

Supporting Information

A Multi-Configurational Wave Function Theoretical Study on Electronic Structure and Magnetic Susceptibility of Dilanthanide Single Molecule Magnet

Yue Chen[1], Ray Miyazaki[1], Shigeyoshi Sakaki[2], and Jun -ya Hasegawa[1,3]*

[1] Institute for Catalysis, Hokkaido University, N21W10, Kita-ku, Sapporo 001-0021, Japan

[2] Institute for Cell-Material Sciences, Kyoto University, Rhom Plaza, Kyoto-daigaku Katsura, Nishikyo-ku, Kyoto 615-8146, Japan

[3] Interdisciplinary Research Center for Catalytic Chemistry, National Institute of Advanced Industrial Science and Technology, Tsukuba 305-8565, Japan

E-mail: hasegawa@cat.hokudai.ac.jp

S1. Computational models and choice of exchange-correlation functionals

Table S1 (A) The geometry of **Ferri** of Gd complex optimzed by different DFT functionals.

	Gd-Gd	N1-N2	Gd-O	Gd-N1	Gd-N2	Gd-N3	Gd-N4	RMSE[a]
(1) Computational model (Figure 1b)								
B3LYP	4.315	1.381	2.552	2.336	2.193	2.340	2.341	0.054
mPW1PW91	4.210	1.387	2.521	2.271	2.160	2.315	2.318	0.044
M06HF	4.210	1.370	2.379	2.204	2.223	2.343	2.343	0.048
BHandHLYP	4.200	1.388	2.480	2.215	2.209	2.353	2.365	0.025
B3PW91	4.274	1.376	2.542	2.312	2.176	2.321	2.325	0.048
CAM-B3LYP	4.588	1.256	2.559	2.374	2.383	2.375	2.354	0.162
ωB97X	4.605	1.259	2.550	2.378	2.395	2.380	2.371	0.168
BHandH	4.165	1.365	2.403	2.193	2.190	2.293	2.319	0.063
ωB97XD	4.170	1.393	2.461	2.200	2.196	2.339	2.349	0.041
M06-2X	4.204	1.394	2.433	2.209	2.220	2.343	2.349	0.032
PBEh1PBE	4.187	1.383	2.467	2.208	2.201	2.337	2.346	0.035
(2) Original compound (Figure 1a)								
BHandHLYP	4.238	1.381	2.524	2.242	2.215	2.365	2.395	0.024
Expt.	4.248	1.400	2.480	2.249	2.224	2.382	2.357	

[a] RMSE is the root mean square error. [b] Units are in Angstrom. [c] See Figure S1 for atom labels

Table S1 (B) The geometries optimzed for **Ferro** and **Ferri** with the BHandHLYP functional.

	Ln1-N1	Ln1-N2	Ln1-O	Ln1-N3	N1-N2
			$[Gd(N_2)Gd]^{1-}$		
Ferro	2.217	2.210	2.481	2.365	1.385
Ferri	2.215	2.209	2.480	2.365	1.388
Expt.	2.249	2.224	2.480	2.382	1.400
			$[Tb(N_2)Tb]^{1-}$		
Ferro	2.202	2.200	2.459	2.350	1.390
Ferri	2.207	2.200	2.461	2.338	1.393
Expt.	2.234	2.206	2.479	2.360	1.394
			$[Dy(N_2)Dy]^{1-}$		
Ferro	2.186	2.186	2.454	2.327	1.400
Ferri	2.186	2.189	2.452	2.328	1.402
Expt.	2.213	2.202	2.455	2.343	1.400

[a] Units are in Angstrom.

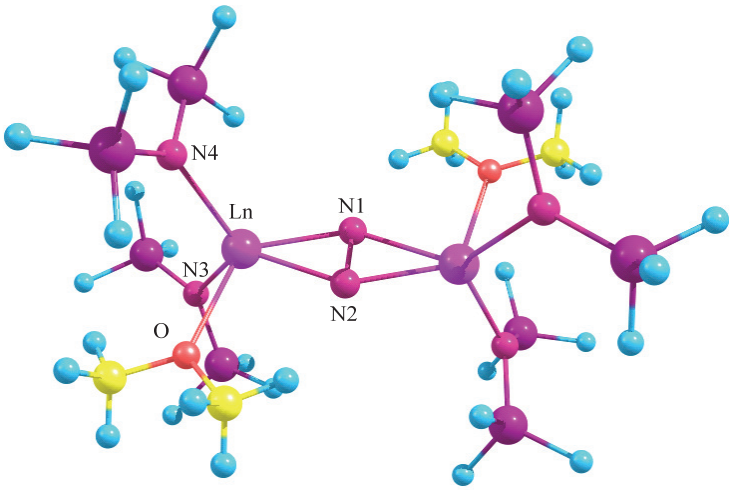

Figure S1. Atomic labels of lanthanide complex $[Ln(N_2)Ln]^{1-}$.

S2. Active space of the dilanthanoid complexes for CASSCF calculations

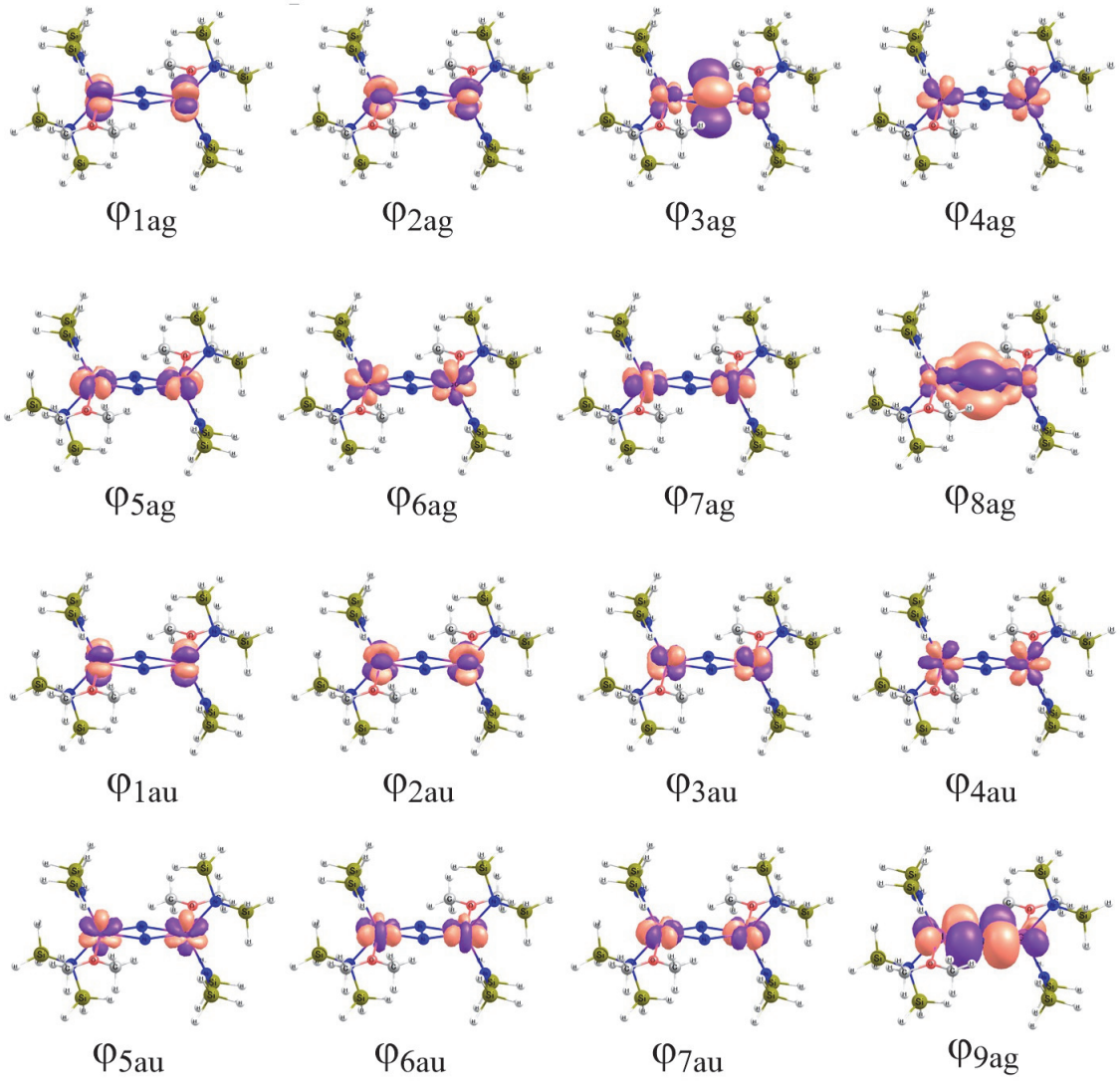

Figure S2(a) CASSCF natural orbitals of $[Gd(N_2)Gd]^{1-}$. Occupation number of φ_{3ag} and φ_{8ag} are 0.93 and 1.07, respectively. That of the other orbitals are 1.00, while φ_{9ag} is 2.00.

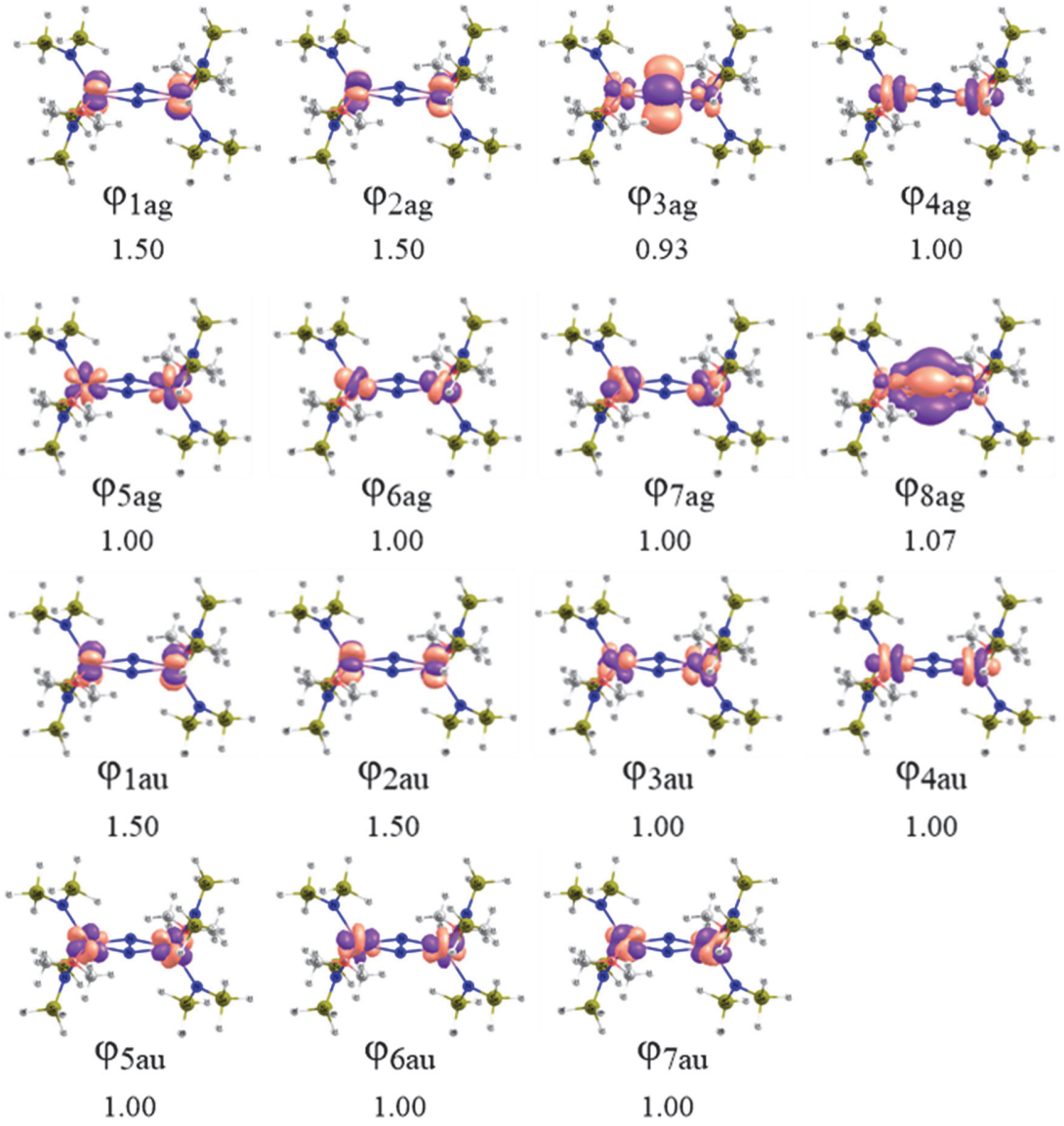

Figure S2(b) CASSCF natural orbitals of $[Tb(N_2)Tb]^{1-}$ and their occupation number.

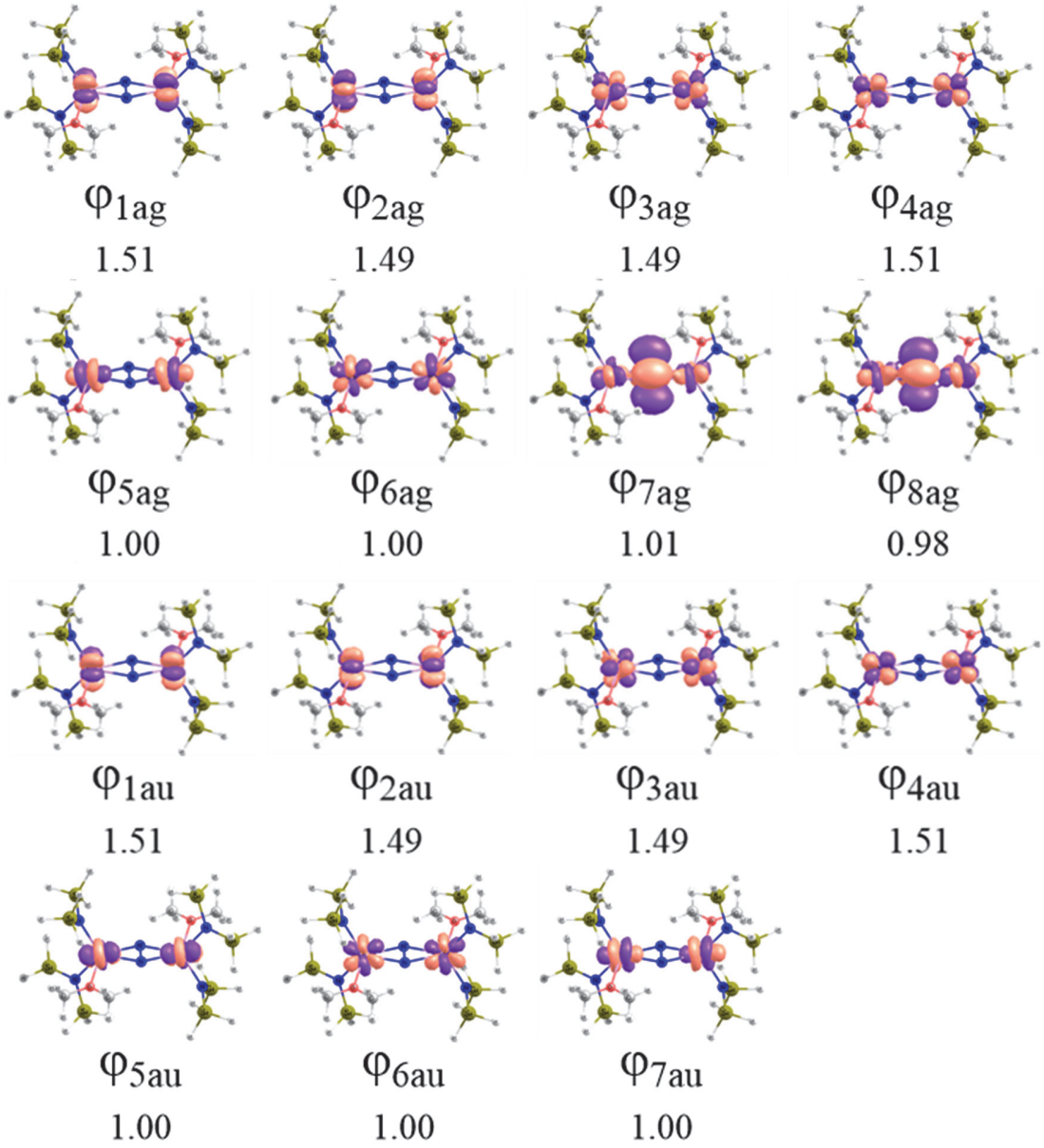

Figure S2(c) CASSCF natural orbitals of $[Dy(N_2)Dy]^{1-}$ and their occupation number.

S3. Relative potential energy of the ground and excited states of the dilanthanoid complexes obtained with MS-CASPT2 calculations.

S3-1. MS-CASPT2 energy for the Gd, Tb, and Dy complexes

Calculated energy levels of the Gd, Tb, Dy dilanthanide complexes were summarized in Tables S2(A, B, and C), respectively. All the transitions are f-f transitions, because the active space is composed of fifteen orbitals including lanthanide 4f orbitals and two N_2 π^* orbitals. See Figure S2 for the distribution of the orbitals.

Table S2 (A). The energies (kcal/mol) of different spin states of Gd complex **1** calculated by MS-CASPT2

	Root 1	Root 2	Root 3	Root 4	Root 5	DFT
^{16}Ag	246.13	248.92	252.16	253.92	254.95	1.57
^{16}Au	0.71	50.82	249.94	256.58	260.84	
^{14}Ag	1.26	108.20	108.53	108.53	125.99	0.00
^{14}Au	**0.00**	108.32	108.65	108.65	126.11	
^{12}Ag	0.24	107.45	108.30	108.62	108.65	97.18
^{12}Au	1.27	107.07	108.19	108.83	108.56	
^{10}Ag	1.18	107.17	108.11	108.43	108.47	278.56
^{10}Au	0.32	107.29	108.19	108.50	108.54	
^{8}Ag	0.41	107.37	108.08	108.38	108.44	356.27
^{8}Au	1.09	107.29	108.02	108.33	108.39	
^{6}Ag	1.04	107.45	107.87	107.98	108.30	292.09
^{6}Au	0.49	107.45	107.98	108.27	108.34	
^{4}Ag	0.61	107.70	107.95	108.15	108.23	498.53
^{4}Au	0.93	107.53	107.87	108.16	108.22	
^{2}Ag	0.90	107.65	107.97	107.99	125.52	522.58

^{2}Au	0.74	107.67	107.99	108.00	125.48

Table S2 (B). The energies (kcal/mol) of different spin states of Tb complex **2** calculated by MS-CASPT2.

	Root 1	Root 2	Root 3	Root 4	Root 5
^{14}Ag	1.448	2.438	2.515	2.566	2.789
^{14}Au	1.442	2.327	2.469	2.859	2.967
^{12}Ag	0.207	1.285	1.555	1.568	2.565
^{12}Au	**0.000**	1.429	2.455	2.492	2.766
^{10}Ag	0.138	1.313	2.377	2.424	2.650
^{10}Au	0.300	1.307	1.479	1.653	2.378
^{8}Ag	0.390	0.500	1.721	1.755	2.202
^{8}Au	0.260	1.188	2.153	2.255	2.523
^{6}Ag	0.692	1.083	1.699	2.064	2.147
^{6}Au	0.481	1.131	1.557	1.831	2.065
^{4}Ag	2.575	1.022	1.645	1.923	1.935
^{4}Au	0.521	0.975	1.912	2.038	2.309
^{2}Ag	0.644	0.869	1.818	1.939	2.210
^{2}Au	0.673	0.899	1.744	7.854	2.019

Table S2 (C). The energies (kcal/mol) of different spin states of Dy complex **3** calculated by MS-CASPT2.

	Root 1	Root 2	Root 3	Root 4	Root 5
^{12}Ag	0.757	1.115	1.135	1.137	1.153
^{12}Au	0.791	0.795	0.808	1.161	1.177
^{10}Ag	**0.000**	0.811	0.818	0.823	1.085
^{10}Au	0.168	0.175	0.179	0.919	1.127
^{8}Ag	0.243	0.249	0.252	0.839	0.921
^{8}Au	0.105	0.741	0.745	0.751	0.882
^{6}Ag	0.199	0.667	0.674	0.677	0.743
^{6}Au	0.294	0.298	0.301	0.740	0.747
^{4}Ag	0.349	0.352	0.354	0.648	0.674
^{4}Au	0.285	0.583	0.597	0.600	0.659
^{2}Ag	0.389	0.536	0.544	0.546	0.562
^{2}Au	0.419	0.421	0.423	0.546	0.575

S3-2. Energy levels of the Full model and simplified model

As shown in Figure 1 of the main text, we reduced our computation model by simplifying the ligand structure. We show that this simplification does not significantly affect the energy levels. In Table S3(D), we compare the energy levels calculated with the original structure

and the simplified structure. CASSCF and CASPT2 methods were adopted for the comparison. The root mean square deviation (RMSE) in the CASSCF and CASPT2 calculations for the $^{14}A_u$, $^{12}A_g$, and $^{10}A_u$ states was 0.14 kcal/mol and 1.45 kcal/mol, respectively. We note that the deviation in the CASPT2 results arose from the highly lying excited state. If the lowest-three states are concerned, only negligible deviation is observed.

Table S3(D). Comparison of CASSCF, CASPT2, MS-CASPT2 energy between the original structure model (Figure 1a) and simplified model (Figure 1b) of the Gd complex. The energy are relative to the lowest $^{14}A_u$ state. Units are in kcal mol^{-1}.

State	$^{14}A_u$		$^{12}A_g$		$^{10}A_u$	
	Original	Model	Original	Model	Original	Model
(1)CASSCF, RMSE = 0.14 kcal/mol						
1	**0.00**	**0.00**	-0.10	-0.13	-0.13	-0.16
2	116.06	115.89	116.12	115.99	116.16	116.02
3	116.14	115.99	116.22	116.05	116.26	116.12
4	116.24	116.03	116.31	116.12	116.35	116.18
5	124.00	123.81	116.53	116.52	116.49	116.47
(2)CASPT2, RMSE = 1.53 kcal/mol						
1	**0.00**	**0.00**	0.23	0.24	0.32	0.32
2	110.29	108.40	110.25	108.34	110.14	108.21
3	110.27	108.65	110.26	108.61	110.14	108.49
4	110.35	108.56	110.32	108.60	110.21	108.52

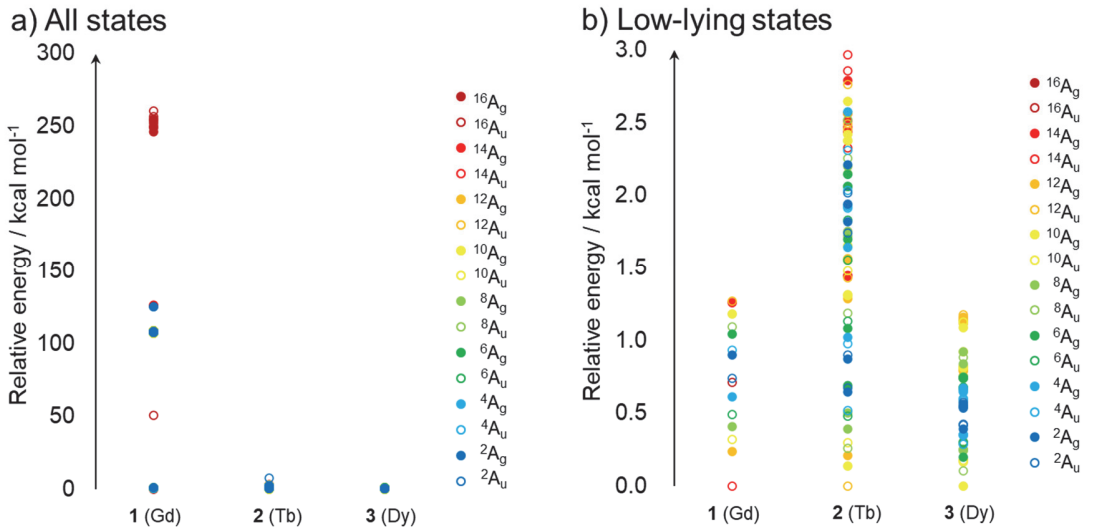

Figure S3 Energy levels of the excited states of **1**, **2**, and **3**. (a) All of the calculated excited states. (b) Low-lying excited states.

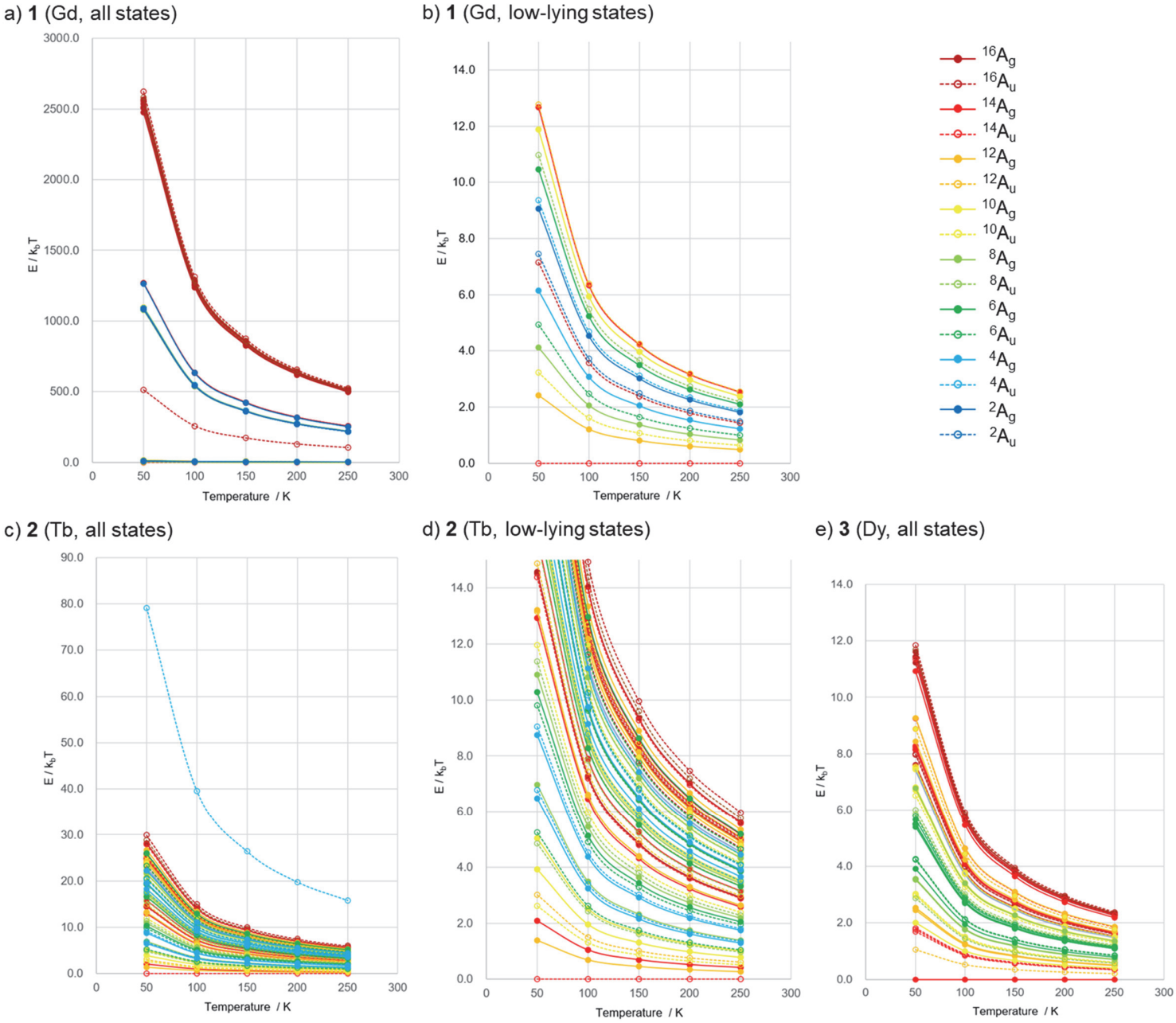

Figure S4. Energy levels of **1**, **2**, and **3** in k_bT unit. Temperature dependence of the E/k_bT values are plotted for (a) **1** (all the calculated states), (2) **1** (low-lying states), (3) **2** (all the calculated states), (d) **2** (low-lying states), (e) **3** (all the calculated states).

S4. Relative potential energy of ferromagnetic coupling state (Ferro) and ferrimagnetic coupling state (Ferri) states of the lanthanoid complexes obtained with Multistate-CASPT2 calculations.

Table S3: Energy gap between **Ferro** and **Ferri** (E_{Ferro}-E_{Ferri}, unit: kcal/mol).

	DFT (BHandHLYP)	CASPT2
1	1.55	0.94
2	-0.41	1.43
3	-0.02	0.76

S5. Saturation magnetization

In the magnetic hysteresis loop, at the maximum field B_{max} (or $-B_{max}$) the powder sample has saturation magnetization (M_{sat}); see Figure S4. Considering the random orientation of the molecule in powder sample, component of magnetic moment along the external field is μ_m•cosθ and the total magnetization along external field may be caluclated by eq. S1:

$$M_{sat} = \int_0^{\pi/2} \mu_m \cos\theta \cdot \sin\theta \, d\theta \cdot = \frac{1}{2}\mu_m \qquad \text{(S1)}$$

where μ_m is the molecular magnetic moment, θ is the angle between external field and the magnetic moment.

This relationship indicates that M_{sat} of powder sample is half of M_{sat} along the easy axis of crystal sample in condition that the gound state is the most populated under a temperature and an applied field.

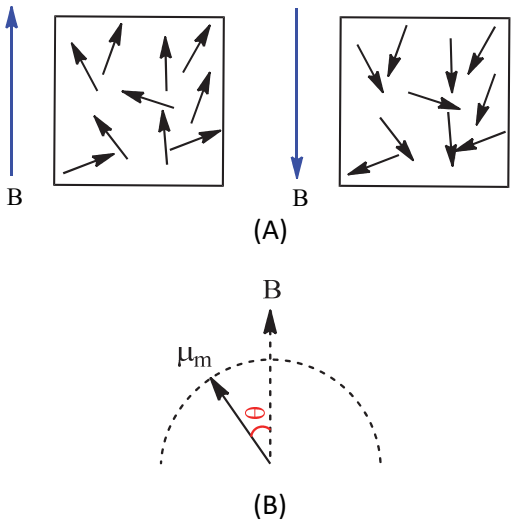

Figure S5. (A)Random molecular orientation at B_{max} or $-B_{max}$, and (B) angle θ between molecule magnetic moment and external field.

S6. Cartesian coordinates of the dilanthanide complexes

$[Gd(N_2)Gd]^{-1}$(Computational model)

GD1	2.031701	0.376893	−0.374837
GD1	−2.031701	−0.376893	0.374837
N1	−0.092701	−0.150196	−0.671135
N1	0.092701	0.150196	0.671135
N2	2.797634	2.380220	−1.370401
N2	−2.797634	−2.380220	1.370401
N3	3.504837	−1.457113	−0.428056
N3	−3.504837	1.457113	0.428056
O1	2.840036	1.283525	1.787360
O1	−2.840036	−1.283525	−1.787360
C1	4.126074	1.840704	1.942826
C1	−4.126074	−1.840704	−1.942826
C2	2.118766	1.172255	3.000493
C2	−2.118766	−1.172255	−3.000493
SI1	3.987371	2.401497	−2.608426
SI1	−3.987371	−2.401497	2.608426
SI2	2.064111	3.827377	−0.796330
SI2	−2.064111	−3.827377	0.796330
SI3	3.406969	−2.110044	−2.007965
SI3	−3.406969	2.110044	2.007965
SI4	4.379776	−2.140780	0.876062
SI4	−4.379776	2.140780	−0.876062

H1	4.759540	1.182347	2.547720
H1	-4.759540	-1.182347	-2.547720
H2	4.552591	1.959647	0.947005
H2	-4.552591	-1.959647	-0.947005
H3	4.056486	2.825493	2.418312
H3	-4.056486	-2.825493	-2.418312
H4	1.141357	0.765984	2.747407
H4	-1.141357	-0.765984	-2.747407
H5	2.646199	0.503827	3.690488
H5	-2.646199	-0.503827	-3.690488
H6	2.010323	2.161466	3.459546
H6	-2.010323	-2.161466	-3.459546
H7	5.271405	3.081631	-2.222751
H7	-5.271405	-3.081631	2.222751
H8	3.558126	3.075695	-3.878315
H8	-3.558126	-3.075695	3.878315
H9	4.361675	1.001491	-2.977992
H9	-4.361675	-1.001491	2.977992
H10	1.462569	4.692499	-1.861838
H10	-1.462569	-4.692499	1.861838
H11	0.970681	3.473754	0.158212
H11	-0.970681	-3.473754	-0.158212
H12	3.001749	4.728792	-0.040700
H12	-3.001749	-4.728792	0.040700
H13	2.449583	-1.213916	-2.751952
H13	-2.449583	1.213916	2.751952
H14	4.678811	-2.108406	-2.799019
H14	-4.678811	2.108406	2.799019
H15	2.860495	-3.499590	-2.112227
H15	-2.860495	3.499590	2.112227
H16	5.872766	-2.072962	0.723320
H16	-5.872766	2.072962	-0.723320
H17	4.074356	-1.401773	2.142399
H17	-4.074356	1.401773	-2.142399
H18	4.080896	-3.584161	1.149300
H18	-4.080896	3.584161	-1.149300

[Tb(N_2)Tb]$^{-1}$(Computational model)

TB	2.073416	-0.262541	-0.039077
TB	-2.073416	0.262541	0.039077
N1	0.041036	0.257900	0.645448
N1	-0.041036	-0.257900	-0.645448
N2	3.538545	1.196996	-1.154457
N2	-3.538545	-1.196996	1.154457
N3	2.947734	-2.355049	0.530530
N3	-2.947734	2.355049	-0.530530
O1	2.825535	0.815666	2.041090
O1	-2.825535	-0.815666	-2.041090
C1	4.188561	0.989909	2.359799

C1	-4.188561	-0.989909	-2.359799
C2	1.946443	1.196942	3.083938
C2	-1.946443	-1.196942	-3.083938
SI1	4.808214	0.648443	-2.172976
SI1	-4.808214	-0.648443	2.172976
SI2	-3.241248	-2.876788	0.923135
SI2	3.241248	2.876788	-0.923135
SI3	2.884914	-3.283024	-0.906942
SI3	-2.884914	3.283024	0.906942
SI4	3.370123	-2.959882	2.077054
SI4	-3.370123	2.959882	-2.077054
H1	4.477046	0.328844	3.184542
H1	-4.477046	-0.328844	-3.184542
H2	4.766137	0.749723	1.467486
H2	-4.766137	-0.749723	-1.467486
H3	4.381247	2.032397	2.636511
H3	-4.381247	-2.032397	-2.636511
H4	0.935428	1.049688	2.708978
H4	-0.935428	-1.049688	-2.708978
H5	2.123161	0.575306	3.968973
H5	-2.123161	-0.575306	-3.968973
H6	2.108405	2.250743	3.337560
H6	-2.108405	-2.250743	-3.337560
H7	6.188235	0.979517	-1.677487
H7	-6.188235	-0.979517	1.677487
H8	-4.760670	-1.183359	3.573948
H8	4.760670	1.183359	-3.573948
H9	4.762561	-0.841929	-2.287446
H9	-4.762561	0.841929	2.287446
H10	-3.121475	-3.670723	2.188416
H10	3.121475	3.670723	-2.188416
H11	-1.964258	-3.049868	0.167526
H11	1.964258	3.049868	-0.167526
H12	-4.299475	-3.578983	0.116940
H12	4.299475	3.578983	-0.116940
H13	2.336391	-2.344992	-1.953635
H13	-2.336391	2.344992	1.953635
H14	4.197391	-3.772437	-1.436181
H14	-4.197391	3.772437	1.436181
H15	1.979617	-4.474148	-0.882457
H15	-1.979617	4.474148	0.882457
H16	4.836300	-3.237363	2.251880
H16	-4.836300	3.237363	-2.251880
H17	3.025996	-1.962017	3.138499
H17	-3.025996	1.962017	-3.138499
H18	2.683074	-4.236401	2.458919
H18	-2.683074	4.236401	-2.458919

$[Dy(N_2)Dy]^{-1}$(Computational model)

DY	2.070492	-0.046684	-0.074588
DY	-2.070492	0.046684	0.074588
N1	0.027620	0.038064	0.699225
N1	-0.027620	-0.038064	-0.699225
N2	3.353804	1.799511	-0.676267
N2	-3.353804	-1.799511	0.676267
N3	3.135206	-2.094857	-0.212038
N3	-3.135206	2.094857	0.212038
O1	2.789141	0.401726	2.226684
O1	-2.789141	-0.401726	-2.226684
C1	4.137736	0.590543	2.594524
C1	-4.137736	-0.590543	-2.594524
C2	1.903271	0.352114	3.330684
C2	-1.903271	-0.352114	-3.330684
SI1	4.594607	1.725089	-1.862650
SI1	-4.594607	-1.725089	1.862650
SI2	-2.951894	-3.283755	-0.099075
SI2	2.951894	3.283755	0.099075
SI3	3.130389	-2.591218	-1.855258
SI3	-3.130389	2.591218	1.855258
SI4	3.670272	-3.085417	1.082105
SI4	-3.670272	3.085417	-1.082105
H1	4.500540	-0.266146	3.173242
H1	-4.500540	0.266146	-3.173242
H2	4.715320	0.693263	1.676240
H2	-4.715320	-0.693263	-1.676240
H3	4.243390	1.507414	3.184945
H3	-4.243390	-1.507414	-3.184945
H4	0.900884	0.234168	2.923191
H4	-0.900884	-0.234168	-2.923191
H5	2.157350	-0.495632	3.976999
H5	-2.157350	0.495632	-3.976999
H6	1.973048	1.283803	3.903489
H6	-1.973048	-1.283803	-3.903489
H7	5.977542	1.972449	-1.328714
H7	-5.977542	-1.972449	1.328714
H8	-4.434779	-2.698753	2.992588
H8	4.434779	2.698753	-2.992588
H9	4.631454	0.362568	-2.476996
H9	-4.631454	-0.362568	2.476996
H10	-2.732316	-4.433772	0.835756
H10	2.732316	4.433772	-0.835756
H11	-1.696613	-3.104864	-0.888143
H11	1.696613	3.104864	0.888143
H12	-3.990845	-3.763322	-1.075472
H12	3.990845	3.763322	1.075472
H13	2.471693	-1.478446	-2.623020
H13	-2.471693	1.478446	2.623020
H14	4.479241	-2.788555	-2.476229

H14	-4.479241	2.788555	2.476229
H15	2.357439	-3.838475	-2.150037
H15	-2.357439	3.838475	2.150037
H16	5.162985	-3.227614	1.173281
H16	-5.162985	3.227614	-1.173281
H17	3.246240	-2.504479	2.394541
H17	-3.246240	2.504479	-2.394541
H18	3.144760	-4.488765	1.049922
H18	-3.144760	4.488765	-1.049922

$[Gd(N_2)Gd]^{-1}$ (Original compound model)

Gd	-0.30724900	-2.09466100	-0.09025200
Si	0.36657300	-5.15383700	1.65586400
Si	1.33774300	-2.59835200	2.98868500
Si	1.44755300	-3.22356900	-2.81717100
Si	-1.55184800	-3.31090800	-3.26908700
O	-2.63937900	-2.22152100	0.86586700
N	0.67881600	-0.11093500	-0.06006400
N	0.47670300	-3.43421800	1.73436600
N	-0.17646300	-2.99602800	-2.27236100
C	2.62320300	-2.99998700	-1.34676200
C	-0.71357100	-5.66899200	0.18614200
C	2.03064700	-6.04208300	1.42960400
C	-0.44819300	-5.98612500	3.16204800
C	1.76296300	-3.63675200	4.52517200
C	2.98421900	-1.88819600	2.37979300
C	0.30472600	-1.15433900	3.63629600
C	2.03139300	-1.98074400	-4.12454600
C	-4.60097300	-1.36138900	1.85235700
C	-3.01553800	-3.10500900	1.93205400
C	-3.89096100	-2.27171400	2.84724000
C	-3.49924800	-1.06043600	0.85166400
C	1.78540700	-4.94875700	-3.53423800
C	-1.38194900	-2.72623400	-5.06665900
C	-3.08034400	-2.44319100	-2.56250200
C	-2.00819100	-5.15146600	-3.38318100
H	3.66383600	-3.08100000	-1.68089900
H	2.47104300	-3.74481200	-0.56018900
H	2.51064200	-2.00889100	-0.89038800
H	1.51915100	-5.73179100	-2.81592200
H	-2.24021000	-5.56472100	-2.39629400
H	-0.36577700	-5.24361100	-0.76005900
H	-1.75745100	-5.36066300	0.32281200
H	-0.71177900	-6.76020800	0.08161100
H	2.50396600	-5.75916200	0.48347200
H	1.89846200	-7.13080800	1.42474000
H	2.73076800	-5.79474200	2.23496900
H	-1.41842200	-5.53390600	3.39703300
H	0.17306000	-5.92364000	4.05961700
H	-0.62183400	-7.04855900	2.95070900

H	0.86420100	-3.96345400	5.05816300
H	2.35149800	-3.02017600	5.21509900
H	2.35776500	-4.52553000	4.28919000
H	2.80205800	-1.18067900	1.56451000
H	3.64291500	-2.67901800	2.00362100
H	3.50999100	-1.35740600	3.18250100
H	0.04750800	-0.45114400	2.83735500
H	0.84626200	-0.59445500	4.40697100
H	-0.62748900	-1.51821400	4.08512700
H	-4.99962500	-0.45035200	2.30268300
H	-5.42773500	-1.89560100	1.37246900
H	-3.57085200	-3.94969400	1.50777800
H	-2.10006600	-3.46878600	2.39571300
H	-3.27036900	-1.68048300	3.52710200
H	-4.56937100	-2.88489100	3.44444600
H	-2.89106700	-0.20228900	1.13461400
H	-3.85809100	-0.91564700	-0.16710900
H	3.09734900	-2.12157600	-4.34313200
H	1.88401600	-0.95595300	-3.76870700
H	1.48056200	-2.08357200	-5.06433700
H	2.84576600	-5.06686600	-3.78783400
H	1.20566900	-5.12438300	-4.44746100
H	-1.12582100	-1.66351100	-5.11795400
H	-2.32489900	-2.87696300	-5.60588000
H	-0.60479000	-3.28387500	-5.60120600
H	-2.93855700	-1.35773900	-2.51780300
H	-3.31062600	-2.79892000	-1.55211000
H	-3.95724900	-2.64153600	-3.18954600
H	-1.18519600	-5.74139200	-3.80069200
H	-2.88500300	-5.29658900	-4.02642100
Gd	0.30724900	2.09466100	0.09025200
Si	-0.36657300	5.15383700	-1.65586400
Si	-1.33774300	2.59835200	-2.98868500
Si	-1.44755300	3.22356900	2.81717100
Si	1.55184800	3.31090800	3.26908700
O	2.63937900	2.22152100	-0.86586700
N	-0.67881600	0.11093500	0.06006400
N	-0.47670300	3.43421800	-1.73436600
N	0.17646300	2.99602800	2.27236100
C	-2.62320300	2.99998700	1.34676200
C	0.71357100	5.66899200	-0.18614200
C	-2.03064700	6.04208300	-1.42960400
C	0.44819300	5.98612500	-3.16204800
C	-1.76296300	3.63675200	-4.52517200
C	-2.98421900	1.88819600	-2.37979300
C	-0.30472600	1.15433900	-3.63629600
C	-2.03139300	1.98074400	4.12454600
C	4.60097300	1.36138900	-1.85235700
C	3.01553800	3.10500900	-1.93205400
C	3.89096100	2.27171400	-2.84724000

C	3.49924800	1.06043600	-0.85166400
C	-1.78540700	4.94875700	3.53423800
C	1.38194900	2.72623400	5.06665900
C	3.08034400	2.44319100	2.56250200
C	2.00819100	5.15146600	3.38318100
H	-3.66383600	3.08100000	1.68089900
H	-2.47104300	3.74481200	0.56018900
H	-2.51064200	2.00889100	0.89038800
H	-1.51915100	5.73179100	2.81592200
H	2.24021000	5.56472100	2.39629400
H	0.36577700	5.24361100	0.76005900
H	1.75745100	5.36066300	-0.32281200
H	0.71177900	6.76020800	-0.08161100
H	-2.50396600	5.75916200	-0.48347200
H	-1.89846200	7.13080800	-1.42474000
H	-2.73076800	5.79474200	-2.23496900
H	1.41842200	5.53390600	-3.39703300
H	-0.17306000	5.92364000	-4.05961700
H	0.62183400	7.04855900	-2.95070900
H	-0.86420100	3.96345400	-5.05816300
H	-2.35149800	3.02017600	-5.21509900
H	-2.35776500	4.52553000	-4.28919000
H	-2.80205800	1.18067900	-1.56451000
H	-3.64291500	2.67901800	-2.00362100
H	-3.50999100	1.35740600	-3.18250100
H	-0.04750800	0.45114400	-2.83735500
H	-0.84626200	0.59445500	-4.40697100
H	0.62748900	1.51821400	-4.08512700
H	4.99962500	0.45035200	-2.30268300
H	5.42773500	1.89560100	-1.37246900
H	3.57085200	3.94969400	-1.50777800
H	2.10006600	3.46878600	-2.39571300
H	3.27036900	1.68048300	-3.52710200
H	4.56937100	2.88489100	-3.44444600
H	2.89106700	0.20228900	-1.13461400
H	3.85809100	0.91564700	0.16710900
H	-3.09734900	2.12157600	4.34313200
H	-1.88401600	0.95595300	3.76870700
H	-1.48056200	2.08357200	5.06433700
H	-2.84576600	5.06686600	3.78783400
H	-1.20566900	5.12438300	4.44746100
H	1.12582100	1.66351100	5.11795400
H	2.32489900	2.87696300	5.60588000
H	0.60479000	3.28387500	5.60120600
H	2.93855700	1.35773900	2.51780300
H	3.31062600	2.79892000	1.55211000
H	3.95724900	2.64153600	3.18954600
H	1.18519600	5.74139200	3.80069200
H	2.88500300	5.29658900	4.02642100